Title: Thermal Decomposition Synthesis of Nanorods Bismuth Sulphide from Bismuth N-ethyl Cyclohexyl Dithiocarbamate Complex

Author: Nurul Hidayah Abdullah Zulkarnain Zainal Sidik Silong Mohamed Ibrahim Mohamed Tahir Kar-Ban Tan Sook-Keng Chang

PII: S0040-6031(16)30023-5
DOI: http://dx.doi.org/doi:10.1016/j.tca.2016.03.001
Reference: TCA 77448

To appear in: *Thermochimica Acta*

Received date: 30-9-2015
Revised date: 28-2-2016
Accepted date: 4-3-2016

Please cite this article as: Nurul Hidayah Abdullah, Zulkarnain Zainal, Sidik Silong, Mohamed Ibrahim Mohamed Tahir, Kar-Ban Tan, Sook-Keng Chang, Thermal Decomposition Synthesis of Nanorods Bismuth Sulphide from Bismuth N-ethyl Cyclohexyl Dithiocarbamate Complex, Thermochimica Acta http://dx.doi.org/10.1016/j.tca.2016.03.001

Thermal Decomposition Synthesis of Nanorods Bismuth Sulphide from Bismuth N-ethyl Cyclohexyl Dithiocarbamate Complex

Nurul Hidayah Abdullah[a,b], Zulkarnain Zainal[a,b*] zulkar@upm.edu.my, Sidik Silong[c],
Mohamed Ibrahim Mohamed Tahir[a], Kar-Ban Tan[a], Sook-Keng Chang[b]

[a]Department of Chemistry, Faculty of Science, Universiti Putra Malaysia, 43400 UPM Serdang, Selangor, Malaysia
[b]Materials Synthesis and Characterization Laboratory, Institute of Advanced Technology, Universiti Putra Malaysia, 43400 UPM Serdang, Selangor, Malaysia
[c]UiTM Negeri Sembilan, Kampus Kuala Pilah, Pekan Parit Tinggi, 72000 Kuala Pilah, Negeri Sembilan, Malaysia

Tel.: +6 03 89464209; fax: +6 03 89464232

Highlights

Bismuth N-ethyl cyclohexyl dithiocarbamate was used as single source precursor.

No surfactant was used in the preparation of Bi_2S_3 nanorods.

Pure phase orthorhombic Bi_2S_3 is obtained.

Bismuth sulphide with an average atomic ratio of Bi:S close to 2:3 is obtained.

Abstract

Nanorods of bismuth sulphide were prepared by thermal decomposition of bismuth N-ethyl cyclohexyl dithiocarbamate at different calcination duration. X-ray diffraction (XRD) analysis shows that at 400 °C, the precursor was fully decomposed to orthorhombic bismuth sulphide after 2 hours of calcination. Besides, calcination duration does not affect the existence of Bi_2S_3 phase. Field emission scanning electron microscopy (FESEM) and transmission electron microscopy (TEM) analyses reveal that Bi_2S_3 nanorods with an average width ranging from 29-36 nm were obtained. Energy dispersive X-ray (EDX) analysis confirmed the atomic ratio of Bi and S close to 2:3, giving a possible composition of Bi_2S_3. Direct band gap energy of Bi_2S_3 decreases from 1.83 eV to 1.54 eV as calcination time increases.

Keywords: Semiconductors; Heat treatment; Nanostructures; Electron microscopy (TEM and SEM)

1. Introduction

The fabrication of semiconductor based devices have gained much attention since the invention of the transistor in 1947 by American physicists and the development of the integrated silicon chip in the 70s which have been of great use in our daily lives. Advanced technological devices have been rapidly develop for man's insatiable need ranging from MP3 players, computers, mobile phones, and nowadays, flat screen televisions such as liquid crystal display (LCD) and light emitting diode (LED). The escalating interest in both academic and industrial fields in semiconductor technology has led to the increase of studies on binary and ternary semiconductor compounds for their potential applications in electronic and photovoltaic devices respectively [1,2].

The development of nanostructured materials has grown rapidly owing to the dramatic changes in properties (electrical, thermal, mechanical, electronic, optical) in nanoscale dimension through control of matter at the 1–100 nm scale which make them different from their bulk [2,3]. The remarkable concern in nanotechnology has led to the development of semiconducting metal sulphide nanomaterials which possess novel spectroscopic and electronic properties that offer great potential for broad range of applications especially in photovoltaics [4], optoelectronic [5], electrochemical sensors [6], and energy conversion and storage [7]. Nanostructures from inorganic, organic and composite materials can be classified into zero dimensional (0D), one dimensional (1D), two-dimensional (2D) and three-dimensional (3D) with sizes down to the nanometer [2,3,7,8]. Several metal sulphides with different shapes and sizes including nanotubes [9], nanorods [10], nanoparticles [11], nanoflakes [12], and nanobelts [13] have been synthesized for the development of diverse electronic nanodevices.

Researchers have demonstrated the synthesis of nanostructured metal sulphides such as NiS, Bi_2S_3, CoS, ZnS, Sb_2S_3, CuS, CdS, and In_2S_3 by various methods [14-21]. Among the remarkable reported semiconductor material, Bi_2S_3 has been given considerable attention in the field of research due to its potential applications in hydrogen storage [22], high-energy batteries [23], catalytic fields [24], optoelectronic nanodevices [25] photodegradation of dyes [26, 27], solar cell [28] and nanomedicine [29]. For instance, Bi_2S_3 nanowires with band gap energy of ~1.33 eV and current density of about 10^5 A/cm^2 has been reported to be a potential candidate for application in field-emission electronic devices [30]. Furthermore, high quality nanorods and nanowires of Bi_2S_3 have been highlighted to be suitable materials for solar energy, optoelectronic and photoelectronic applications [25,31]. Besides, there is a report about the synthesis of orthorhombic Bi_2S_3 nanoparticles as a photocatalyst for removal of methylene blue dye [32]. Bao *et al.* [25] studied on photoswitchable conductivity of Bi_2S_3 nanowires. From the findings, it was found that the nanowire Bi_2S_3 exhibit nonlinear current-voltage (I-V) characteristics and excellent photoresponse which could be used in optoelectronic nanodevices. In addition, Bi_2S_3 nanorods also have been reported as an ideal agent for in vivo photothermal ablation of tumors and effective tumor metastasis inhibition [29].Furthermore, Bi_2S_3 nanorods incorporated with poly(3-hexylthiophene) (P3HT) have been investigated as new candidate for the fabrication of low-cost and environmentally friendly polymer/inorganic hybrid solar cells [28]. Besides, the incorporation of Bi_2S_3 nanoparticles with TiO_2 has been highlight to have crucial roles in improving the photocatalytic activity for the degradation of methyl orange under visible irradiation [26]. In addition, Bi_2S_3 nanostructures also have been reported to have high efficiency in the photodegradation of rhodamine B (RhB) [27].

Various methods have been employed for the preparation of bismuth sulphides such as refluxing method [33], solvothermal [16,34,35], hydrothermal [17,26], molten salt solvent strategy [36], sonochemical [37], single diffusion method [38], ionic liquid-assisted templating route [39], hot injection technique [27], chemical precipitation [40], in situ thermal sulfuration method [41], microwave irradiation [42,20], solventless synthesis [43,44] and thermal decomposition of single source precursor [45,46]. Among these methods, thermal decomposition of single source precursor is one of the most anticipating techniques to be explored due to the simplicity and different types of precursor have different features which can be exploited for synthesis of nanomaterials with different properties than their bulk counterparts. Wang et al. [44] also reported about the influence of the length of the alkyl group of the precursor on the size of the nanoproduct. They emphasized that precursor with shorter alkyl group yields larger rods of Bi_2S_3.

Metal dithiocarbamate has been widely studied as single source precursor for the preparation of metal sulphide [47,48,49]. Thermal decomposition (thermolysis or pyrolysis) of single source precursors are proven to provide easier and simpler control of the shapes and sizes, and growth of high quality nanoparticles in large scale production [11,14,48]. The preparation of metal dithiocarbamates has been extensively reported by facile reaction between metal salt with carbon disulphide and secondary amine in ethanol or methanol solution [50-54]. Thermal decomposition of organometallic precursors can be done by simply heating the precursors at high temperature in sealed furnace or in high boiling point of solvent to break down the compound into metal sulphide [11,55]. The utilization of single source precursors for preparation of metal sulphides offer several advantages owing to the synthesis process can be conducted under anaerobic condition which is important due to some groups of II-VI and III-V are air sensitive [56]. Furthermore, the use of volatile, toxic and/or pyrophoric precursors also can be avoided. Besides, the utilization of one volatile precursor may cause the purification process to be handled easily than that of two or more volatile precursors that most likely to contribute to the existence of impurities in the nanoparticles. In addition, low temperature deposition routes are also possible for the production of semiconductor nanoparticles. Hence, these factors can affect the optical properties of the compound relative to the predicting optical properties owing to the difference in sizes and shapes of the particles [56].

Herein, bismuth N-ethyl cyclohexyl dithiocarbamate was used as single-source precursor for the preparation of bismuth sulphide via thermal decomposition method at 400 °C. The synthesized bismuth dithiocarbamate was subjected to different calcination duration and the obtained bismuth sulphide will be investigated on its structural, morphological, compositional and band gap properties.

2. Experimental Methods

2.1 Preparation and Characterization of Bismuth Dithiocarbamate

Preparation of Bi(III) complex of N-ethyl cyclohexyl dithiocarbamate was achieved by in-situ reaction of corresponding metal salt with carbon disulphide and potassium hydroxide in cold ethanolic solution of secondary amine. Stoichiometric mol ratio of metal to ligand 1:3 was prepared. Carbon disulphide (0.063 mol) and N-ethylcyclohexylamine (0.063 mol) were added sequentially into ethanolic solution of potassium hydroxide (0.063 mol) and stirred for an hour at 0−4 °C. After an hour of stirring, bismuth(III) chloride (0.021 mol) was added and stirred for another two hours. Dark yellowish orange precipitates was formed and then filtrated and washed thoroughly with distilled water and cold ethanol followed by drying. Recrystallization in chloroform and ethanol solutions yielded pure crystalline material of $C_{27}H_{48}N_3S_6Bi$.

The infrared spectrum of sample was recorded by Universal Attenuated Total Reflection (UATR) technique on a Perkin Elmer 100 Series FT-IR Spectrometer. The spectrum was analyzed in the range of 280-4000 cm^{-1} using liquid nitrogen as carrier gas at room temperature to verify the presence of functional groups in the synthesized compound. Elemental analysis (C, H, N and S) was carried out on a LECO CHNS-932 instrument. The percentage of bismuth content was determined by Optima 7300 DV Optical Emission Spectrometer (OES). Mass spectrum was recorded using Shimadzu Gas Chromatograph-Mass Spectrometer (GCMS-QP5050A) using direct injection (DI-MS) technique to verify the purity and molecular weight of the compound. Thermogravimetric analysis/ differential gravimetric **(**TGA/DTG) analyses were carried out using Mettler Toledo Thermal Gravimetric Analyzer (TGA/SDTA 851e). The sample was analyzed from ambient to 600 ºC in nitrogen atmosphere with the heating rate of 10 ºC min^{-1} to determine decomposition temperature and weight loss of the material. Differential scanning calorimetry (DSC) spectrum was recorded using DSC 7 (Perkin Elmer) equipped with liquid nitrogen cooling system. The sample was analyzed from 0 ºC to 450 ºC in nitrogen atmosphere with the heating rate of 10 ºC min^{-1} to determine the thermodynamic events such as melting point and decomposition temperature.

2.2 Preparation and Characterization of Bismuth Sulphide

Bismuth dithiocarbamate was placed in porcelain crucible in the sealed tubular furnace. The furnace was purged for 15 minutes with nitrogen gas to remove oxygen. Then, the sample was heated at temperature 400 ºC and different calcination duration of 2, 4 and 6 hours in nitrogen atmosphere. The rate of heating was set to 5 ºC min^{-1}. The sample was cooled down before it was taken out from the furnace to prevent the oxidation of the compound. The products were characterized by powder XRD, FESEM, EDX, TEM, and UV-VIS-NIR.

The phase and structure analysis were carried out using the Shidmazu Model XRD-6000 Diffractometer with CuK_α ($\lambda = 1.5418Å$) radiation, employing sampling width of 0.02° in the range from 10 to 80°. The accelerating voltage and current were 30 kV and 30 mA respectively. The morphologies of the samples were studied by JSM-7600F JEOL FESEM attached with energy dispersive X-ray (EDX) analyzer. The chemical compositions were determined by EDX analysis. A Hitachi H-7100 TEM was used to examine the morphology and the particle sizes of the prepared sample. The diffuse reflectance spectra of the as synthesized powders were recorded at room temperature using the Shimadzu UV-3600 Ultraviolet-visible-near infrared (UV-VIS-NIR) spectrophotometer.

3. Results and Discussion

3.1 Synthesis of Bismuth Dithiocarbamate

The reaction of CS_2 with secondary N-ethyl cyclohexylamine in the presence of aqueous KOH leads to the formation of potassium N-ethyl cyclohexyl dithiocarbamate. Bismuth dithiocarbamate (Bi-DTC) was obtained by the reaction of the ligand and bismuth chloride with mol ratio of 3:1. A general reaction scheme for the above preparation is given in Fig. 1.

The C, H, N, S and Bi elemental analyses data show good agreement between the experimental and theoretical percentage based on the suggested molecular formula (Table 1). The synthesized Bi-DTC displays metal:ligand ratio of 1:3 (metal:ligand). High percentage yield of 96% indicates that the in situ chemical reaction is suitable for the preparation of this compound. The physical data and elemental analysis of Bi-DTC is listed in Table 1.

3.2 Fourier Transform Infrared Spectroscopy Analysis

Analysis by infrared spectroscopy was performed to gather the information on the presence of the functional groups. Fig. 2 shows the spectrum of Bi-DTC obtained in the range of 4000-280 cm^{-1}. The three main regions of interest in dithiocarbamate compounds are primarily correlated to v(C—N) of NCS_2^- that appears in the range of 1580–1450 cm^{-1}; the 1060–940 cm^{-1} region which is associated with asymmetric v(C—S) of CSS; and the 420–250 cm^{-1} region that assigned to v(M—S) bond [57-60]. All the main regions that correlated to dithiocarbamate compounds are observed from the spectrum at wavelength 1469, 1007, 360 cm^{-1} for v(C—N), v(—CSS) and v(M—S) respectively. The energy of the the v(C—N) band obtained by bismuth complex can be correlated with the intermediate between the stretching frequencies of single (1250–1360 cm^{-1}) and doubly (1640–1690 cm^{-1}) bonded carbon and nitrogen, suggesting the partial double bond character of the prepared compound [61]. From IR spectrum, the two bands observed at 1007 and 987 cm^{-1} indicate the monodentate character of Bi-DTC. The presence of only one band in the 1000±70 cm^{-1} region is attributed to bidentate character; meanwhile the splitting of the same band in the same region is attributed to monodentate character [58,62]. According to Sarwar *et al.* [63] a split band indicates an asymmetrically bonded bidentate ligand (Δv<20 cm^{-1}) or a monodentate bound ligand (Δv>20 cm^{-1}). The splitting peaks of bismuth complexes in this region also have been reported before [50,64]. The appearance of absorption band at 2928 cm^{-1} was attributed to the v(C-H) stretching for the methyl group [58].

3.3 Mass Spectral Analysis of Bismuth Dithiocarbamate

Mass spectral analysis was performed to determine the molecular weight and fragmentation patterns of Bi-DTC. Fig. 3 shows the mass spectrum of Bi-DTC. Molecular ion that is related to the molecular weight of the proposed molecular formula, $[BiC_{27}H_{48}N_3S_6]^{+\bullet}$ is not found. This can be resulted from either pyrolytic decomposition because of the relatively high temperature is used or due to the fragmentation of the molecular ion in the ionization chamber [65]. Similar observation also has been reported from another mass spectral analysis of bismuth dithiocarbamates with different types of ligands .They also found the fragmentation of $[Bi(S_2CNR_2)_2]^+$ as the parent ion in their mass spectra with no observation of $[Bi(S_2CNR_2)_3]^+$ [46,66] . Based on the mass spectrum analysis, peak corresponds to higher value of 613 m/z can be denoted as direct fragments of the molecular ions with the formula of $[Bi(S_2CNC_8H_{16})_2]^+$ attributed to the loss of one attached ligand from the proposed molecular formula, $[Bi(S_2CNC_8H_{16})_3]$. The observed molecular ion peak is corresponded to the formation of polynuclear compounds from the pyrolytic decomposition of the complexes, during which condensation reactions took place [65]. The base peak observed in the mass spectra is varied depending on the temperature of the ionization chamber and the type of an amine group of the dithiocarbamate ligand. The base peak may correspond either to the $[R_2NCS]^+$ or to the $[CS_2]^+$ ion [65]. Bi-DTC shows mass spectrum with molecular ion peak at 170, 88, and 55 m/z that attribute to the cleavage of $[C_8H_{16}NCS]^+$, $[C_3H_6NS]^+$ and $[C_4H_7]^+$ respectively. The fragment ion mass at 411 m/z was due to the cleavage of $[BiS_2CNC_8H_{16}]^+$. This analysis can provide useful information to support the proposed molecular formula as obtained by elemental composition analysis. Table 2 summarizes the value of molecular ion peaks for selected mass spectral fragments of bismuth dithiocarbamate.

3.4 Thermal Analysis of Bismuth Dithiocarbamate

Thermal behaviour of metal complexes was studied by TGA, DTG and DSC in the presence of nitrogen gas. The summary of thermal analysis results are presented in Table 3. TGA and DTG were investigated by heating the Bi-DTC from ambient to 600 ºC with the heating rate of 10 ºC min^{-1}. The first stage (76-192 °C) is a consecutive step that maximized at 122 °C and 142 °C as shown in the DTG curve (Fig. 4), which could be attributed to the removal of three ethyl groups with weight loss of 11.69 % (calculated 10.67 %) (Table 3). The decomposition of the remaining organic part of Bi-DTC with weight loss of 56.69% (calculated 57.80%) was observed at the temperature of 211-346 °C with DTG peak of 307 °C. The formation of Bi_2S_3 as residue was observed after heat treatment with percentage of residue found is 31.62 % (calculated 31.53 %). No further change is apparent until 600 °C and this indicates the stability of bismuth sulphide up to this temperature without further change to metal oxide. This result is in agreement with the other finding that highlights on the formation of Bi_2S_3 as residue after undergoing thermal treatment of metal complex under nitrogen flow [67]. DSC thermogram (Fig. 5) shows the existence of two endothermic peaks at 127 °C and 157 °C, which could be assigned to the consecutive release of ethyl groups. The sharp endothermic peak was observed at 178 °C attribute to the phase transition. Broad endothermic hump between 292-304 °C was observed due to the decomposition of remaining part of organic moiety to give Bi_2S_3 as residue which is consistent with the TGA analysis.

3.5 Structural Study of Bismuth Sulphide

The crystalline structures of the bismuth sulphides were examined by X-ray diffraction analysis. By changing the calcination duration from 2 to 6 hours at 400 °C, no significant change on the sample phases can be observed. The XRD pattern remains similar except for a slight change in the peak intensity. Sharp diffraction line displays in Fig. 6 reveals the crystalline form of Bi_2S_3. Besides, all the diffraction peaks can be indexed as orthorhombic phase of Bi_2S_3 (ICDD File no. 017-0320; a = 11.1490 Å, b =11.3040 Å, c = 3.9810Å, $\alpha = \beta = \gamma = 90°$). The XRD pattern of the Bi_2S_3 nanoparticles exhibits prominent peaks at scattering angles (2θ) of around 25°, 28.5° and 32° which could be indexed to (130), (211), and (211) planes respectively. Therefore, it is proven that pure orthorhombic Bi_2S_3 can be obtained via thermal decomposition of Bi-DTC at 400 °C. There is no existence of Bi_2O_3 or impurities in the prepared samples. Based on the Debye Scherrer equation [68], the crystallite size is found to increase from approximate 21 nm to 26 nm as calcination duration increases from 2 to 6 hours (Table 4).

3.6 Morphological and Compositional Studies

Bismuth sulphides prepared by thermal decomposition of Bi-DTC at 400 °C were analyzed by FESEM and TEM. FESEM images display the formation of Bi_2S_3 nanorods. Fig. 7 shows a mixture of short and long nanorods of Bi_2S_3 obtained after calcination from 2 to 6 hours. Different calcination duration does not affect the morphology of the sample except for a slight change in the particle size. The particle size distribution (Figure 8) show that the average width of Bi_2S_3 between 29-36 nm. From table 4, the difference between the average crystallite sizes and particle width are shown. Different sizes of Bi_2S_3 are observed due to the non uniform formation of Bi_2S_3 and overlapping of particles caused by the agglomeration. Besides, the particle may compose of two or more individual crystallites. Moreover, the estimation of crystallite sizes by Debye Scherer Equation is generally consistent with TEM analysis for determination of nearly spherical particles rather than nanorod shapes. From this study increased in calcination duration results to the formation of large sizes of Bi_2S_3 nanorods. Other study also highlight the formation of large size of Bi_2S_3 nanostructures with increased in reaction time [46]. Chen *et al.* [69] have reported on the formation of well crystallized Bi_2S_3 nanorods with particle size ranging from 15-90 nm prepared from bismuth citrate by reflux reaction in dimethylformamide (DMF) at 160 °C in the presence of cetyltrimethylammonium bromide (CTAB) as a capping agent. In contrast to their results, Bi_2S_3 nanorods are obtained without using capping agent and DMF in this work. Energy dispersive X-Ray (EDX) analysis was performed for the quantitative analysis of Bi_2S_3 as shown in Fig. 9. The typical EDX spectrum depicts the average atomic ratio of Bi:S close to 2:3, indicating of good stoichiometric sample. Wang *et al.* [44] have discussed about the formation of Bi_2S_3 nanorod. Based on the study, they find that (001) planes have the fastest growth velocity due to highest surface energy. During the ripening process, big Bi_2S_3 particles preferred to grow into rods along [001] direction by consuming small particles. Furthermore the Bi_2S_3 nanorods grown along the c axis are rather stable thermodynamically or kinetically. This explains well why the Bi_2S_3 nanorods prefer to grow along the c axis instead of the b or a axes. Furthermore there is also a report about when unstable nanodots assembled in a line, and with prolonged heating time, the attachment and recrystallization occurred, resulting in the formation of nanorods [46].

3.7 Band Gap Analysis

Band gap values of the prepared samples were determined by diffuse reflectance spectra. Fig. 10 displays Kubelka–Munk transformed reflectance spectra of bismuth sulphides. The band gap of the materials were determined from the plotted of $(F(R)hv)^2$ vs hv. F(R) is Kubelka-Munk function where, $F(R)=(1-R)^2/2R$, R is experimentally observed reflectance [70,71]. The energy intercept of a plot of $(F(R)hv)^2$ versus hv gives direct band gap value when the linear region is extrapolated to the zero ordinate [71]. The band gap energy of Bi_2S_3 decreases as longer calcination duration was set from 2 to 6 hours. The obtained band gap values are around 1.83, 1.56 and 1.54 eV for 2, 4 and 6 hours of calcination duration respectively. These values are slightly higher than that of the reported band gap of Bi_2S_3 (1.3 eV) [44,72]. Wang *et al.* [44] have reported on the direct band gap of 1.5 eV for Bi_2S_3 nanorods. The blue shift might be ascribed to the quantum size effect due to the high aspect ratio of the nanorods relative to the bulk orthorhombic Bi_2S_3 [44]. It can be concluded that shorter calcination duration of 2 hours results to the formation of nanorods Bi_2S_3 with smaller particle sizes and higher band gap energy.

Conclusion

Bismuth sulphide nanorods were successfully synthesized via thermal decomposition of bismuth N-ethyl cyclohexyl dithiocarbamate complex under nitrogen gas flow. Thermal decomposition of Bi-DTC at different calcination duration of 2, 4 and 6 hours at 400 °C yielded high purity orthorhombic Bi_2S_3. The XRD analysis also supported that the calcination of Bi-DTC from 2 to 6 hours may lead to the formation of orthorhombic Bi_2S_3. Different calcination duration did not provide significant effect on the sample phases except for a slight change in the peak intensities and particle sizes. The observed band gap were in the range of 1.54 to 1.83 eV and this indicates blue shift if compared to the bulk sample (1.3 eV). Longer calcination duration resulted in decrement of band gap energy. Besides, EDX analysis confirmed the presence of Bi to S close to ratio 2 : 3 which correspond to the formation of Bi_2S_3. This study shows that thermal decomposition of Bi-DTC at calcination duration from 2 to 6 hours able to generate nanosized bismuth sulphides, suggesting promising applications in electronic and solar cell devices.

Acknowledgements

Financial support from the Research University Grant Scheme of UPM (RUGS 05-01-09-0814RU) is highly appreciated.

References

[1] M.D. Jeroh, D.N. Okoli, Optical and structural properties of amorphous antimony sulphide thin films: effect of dip time, Adv. Appl. Sci. Res. 3 (2012) 793–800.

[2] P. Moriarty, Nanostructured materials, Rep. Prog. Phys. 64 (2001) 297–381.

[3] Deepshikha, T. Basu, A review on synthesis and characterization of nanostructured conducting polymers (NSCP) and application in biosensors, Anal. Lett. 44 (2011) 1126-1171.

[4] W. Yue, W. Cyrus, M. Wanli, S. Bryce, A.P. Alivisatos, Synthesis and photovoltaic application of copper(I) sulfide nanocrystals, Nano Lett. 8 (2008) 2551-2555.

[5] A. Cao, Z. Liu, S. Chu, M. Wu, Z. Ye, Z. Cai, Y. Chang, S. Wang, Q. Gong, Y. Liu, A facile one-step method to produce graphene–CdS quantum dot nanocomposites as promising optoelectronic materials, Adv. Mater. 22 (2010) 103–106.

[6] Q.X. Wang, F. Gao, S. Xing, W. Weng, Z. Shui, Preparation of cauliflower-like bismuth sulfide and its application in electrochemical sensor, Chin. Chem. Lett. 19 (2008) 585–588.

[7] C. Lai, M. Lu, L. Chen, Metal sulfide nanostructures: synthesis, properties and applications in energy conversion and storage, J. Mater. Chem. 22 (2012) 19–30.

[8] J. Zhou, G. Bian, Y. Zhang, Q. Zhu, C. Li, J. Dai, One-dimensional indium sulfides with transition metal complexes of polyamines, Inorg. Chem. 46 (2007) 190–192.

[9] X. Shuai, W. Shen, A facile chemical conversion synthesis of Sb_2S_3 nanotubes and the visible light-driven photocatalytic activities, Nanoscale Res. Lett. 7 (2012) 199−206.

[10] S. Ariponnammal, T. Srinivasan, Growth and characterization of cobalt sulphide nanorods, Res. J. Recent. Sci. 2 (2013) 102–105.

[11] Y.K. Jung, J.I. Kim, J. Lee, Thermal decomposition mechanism of single-molecule precursors forming metal sulfide nanoparticles, J. Am. Chem. Soc. 132 (2010) 178–184.

[12] Y. Liu, M. Zhang, Y. Gao, R. Zhang, Y. Qian, Synthesis and optical properties of cubic In_2S_3 hollow nanospheres, Mater. Chem. Phys. 101 (2007) 362–366.

[13] B.X. Fang, Y. Bando, M. Liao, U.K. Gautam, C. Zhi, B. Dierre, B. Liu, Z. Tianyou, S. Takashi, K. Yasuo, D. Golberg, Single-crystalline ZnS nanobelts as ultraviolet-light sensors, Adv. Mater. 21 (2009) 2034–2039.

[14] I.J. Plante, T.W. Zeid, P. Yang, T. Mokari, Synthesis of metal sulfide nanomaterials via thermal decomposition of single-source precursors, J. Mater. Chem. 20 (2010) 6612–6617.

[15] D.Q. Wang, D.R. Chen, X.L. Jiao, Synthesis of nickel sulfide particles by solvothermal process, Chin. Chem. Lett. 15 (2004) 79–82.

[16] F. Wei, J. Zhang, L. Wang, Z.–K. Zhang, Solvothermal growth of single-crystal bismuth sulfide nanorods using bismuth particles as source material, Cryst. Growth Des. 6 (2006) 1942–1944.

[17] P.K. Panigrahi, Amita Pathak, The Growth of Bismuth Sulfide Nanorods from Spherical-Shaped Amorphous Precursor Particles under Hydrothermal Condition, J. Nanopart. (2013) Article ID 367812,11pages.

[18] L.P. Deshmukh, S.T. Mane, Liquid phase chemical deposition of cobalt sulphide thin films: growth and properties, Dig. J. Nanomater. Biost. 6 (2011) 931–936.

[19] H. Moon, C. Nam, C. Kim, B. Kim, Synthesis and photoluminescence of zinc sulfide nanowires by simple thermal chemical vapor deposition, Mater. Res. Bull. 41 (2006) 2013–2017.

[20] J. Wu, F. Qin, G. Cheng, H. Li, J. Zhang, Y. Xie, H.J. Yang, Z. Lu, X.Yu and R. Chen, Large-scale synthesis of bismuth sulfide nanorods by microwave irradiation, J. Alloy Compd. 509 (2011) 2116–2126.

[21] S.A. Levi, O. Palchik, V. Palchik, M.A. Slifkin, A.M. Weiss, A. Gedanken, Sonochemical synthesis of nanophase indium sulfide, Chem. Mater. 13 (2001) 2195–2200.

[22] Q. Wang, X. Wang, W. Lou, J. Hao, Ionothermal synthesis of bismuth sulfide nanostructures and their electrochemical hydrogen storage behaviour, New J. Chem. 34 (2010) 1930–1935.

[23] X. Zhu, J. Ma, Y. Wang, J. Tao, B. Lin, Y. Ren, X. Jiang, J. Liu, Morphology-controlled synthesis and characterization of bismuth sulfide crystallites via a hydrothermal method, Ceram. Int. 34 (2008) 249–251.

[24] J.M. Zhu, K. Yang, J.J. Zhu, G.B. Ma, X.H. Zhu, S.H. Zhou, Z.G. Liu, The microstructure studies of bismuth sulfide nanorods prepared by sonochemical method, Opt. Mater. 23 (2003) 89–92.

[25] H. Bao, X. Cui, C.M. Li, Y. Gan, J. Zhang, J. Guo, Photoswitchable semiconductor bismuth sulfide (Bi_2S_3) nanowires and their self-supported nanowire arrays, J. Phys. Chem. C 111 (2007) 12279–12283.

[26] J. Lu, Z. Wang, Y. Zhang, X. Zhou, Hydrothermal Synthesis of Bi_2S_3 Nanorods from a Single-Source Precursor and Their Promotional Effect on the Photocatalysis of TiO_2, J. Nanomater. (2013) Article ID 125409 (6 pages).

[27] T. Wu, X. Zhou, H. Zhang, X. Zhong, Bi_2S_3 Nanostructures: A New Photocatalyst, Nano Res. 3 (2010) 379–386.

[28] H.C. Liao, M.C. Wu, M.H. Jao, C.M. Chuang, Y.F. Chen, W.F. Su, Synthesis, optical and photovoltaic properties of bismuth sulfide nanorods, CrystEngComm 14 (2012) 3645-3652.

[29] J. Liu, X. Zheng, L. Yan, L. Zhou, G. Tian,W. Yin, L. Wang, Y. Liu, Z. Hu, Z. Gu,C. Chen, Y. Zhao, Bismuth Sulfide Nanorods as a Precision Nano medicine for in Vivo Multimodal Imaging-Guided Photothermal Therapy of Tumor, J. Am. Chem. Soc. 9 (2015) 696–707.

[30] Y. Yu, C.H. Jin, R.H. Wang, Q. Chen, L.M. Peng, High-quality ultralong Bi_2S_3 nanowires: structure, growth and properties, J. Phys. Chem. B 109 (2005) 18772–18776.

[31] W. Lou, M. Chen, X. Wang, W. Liu, Novel single-source precursors approach to prepare highly uniform Bi_2S_3 and Sb_2S_3 nanorods via a solvothermal treatment, Chem. Mater. 19 (2007) 872–878.

[32] G.O. Siqueira, A. de O. Porto, M.M. Viana, H.V. da Silva, Y.G. de Souza, H.W.A. da Silva, G.M. de Lima, T. Matencio, Bismuth sulphides prepared by thermal and hydrothermal decomposition of a single source precursor: the effect of reaction parameters on morphology, microstructure and catalytic activity, Phys. Chem. Chem. Phys. 15 (2013) 16236–16241.

[33] J. Wu, F. Qin, F.Y.F. Chan, G.Cheng, H. Li, Z. Lu, R. Chen, Fabrication of three-dimensional snowflake-like bismuth sulfide nanostructures by simple refluxing, Mater. Lett. 64 (2010) 287–290.

[34] J. Zhong, W. Xiang, L. Liu, X. Yang, W. Cai, J. Zhang, X. Liang, Biomolecule-assisted Solvothermal Synthesis of Bismuth Sulfide Nanorods, J. Mater. Sci. Technol. 26 (2010) 417-422.

[35] T. Ding, J. Dai, J. Xu, J. Wang, W. Tian, K. Huo, Y. Fang, C. Chen, 3D Hierarchical Bi_2S_3 Nanostructures by Polyvinylpyrrolidone (PVP) and Chloride Ion-Assisted Synthesis and Their Photodetecting Properties, Nanoscale Res. Lett. 10 (2015) 286.

[36] Y. Xi, C. Hu, X. Zhang, Y. Zhang, Z.L. Wang, Optical switches based on Bi_2S_3 nanowires synthesized by molten salt solvent method, Solid State Commun. 149 (2009) 1894-1896.

[37] H. Wang, J.J. Zhu, J.M. Zhu, H.Y. Chen, Sonochemical Method for the Preparation of Bismuth Sulfide Nanorods, J. Phys. Chem. B 106 (2002) 3848-3854.

[38] T. K. Patil, Thermal behavior of semiconductor bismuth tri-sulphide [Bi_2S_3] crystals grown by silica gel, Adv. Appl. Sci. Res. 4 (2013)115-122.

[39] J. Jiang, S.H. Yu, W.T. Yao, H. Ge, G.Z. Zhang, Morphogenesis and Crystallization of Bi_2S_3 Nanostructures by an Ionic Liquid-Assisted Templating Route: Synthesis, Formation Mechanism, and Properties, Chem. Mater. 17 (2005) 6094-6100.

[40] S. Ranjitha, S. Vadivel, D.G. Rajarajan, J. Marimuthu, S. Natarajan, Structural and Optical Properties of Bismuth Sulfide Nanoparticles, Int. J. Sci. Res. (IJSR) (2014) 2319-7064.

[41] Z. Cui, S. Li, J. Zhou, J. Zhang, S. Ge, Z. Zheng, Preparation and Optical Properties of Spherical Bi_2S_3 Nanoparticles by In Situ Thermal Sulfuration Method, NANO: Brief Reports and Reviews 10 (2015) 1550021 (6 pages).

[42] X.H. Liao, H. Wang, J.J. Zhu, H.Y. Chen, Preparation of Bi_2S_3 nanorods by microwave irradiation, Mater. Res. Bull. 36 (2001) 2339 –2346.

[43] M.B. Sigman, Jr., B.A. Korgel, Solventless Synthesis of Bi_2S_3 (Bismuthinite) Nanorods, Nanowires, and Nanofabric, Chem. Mater. 17 (2005)1655-1660.

[44] Y. Wang, J. Chen, P. Wang, L. Chen, Y. Chen, L. Wu, Syntheses, growth mechanism, and optical properties of [001] growing Bi_2S_3 nanorods, J. Phys. Chem. C 113 (2009) 16009–16014.

[45] L. Tian, H.Y. Tan, J.J. Vittal, Morphology-Controlled Synthesis of Bi_2S_3 Nanomaterials via Single and Multiple-Source Approaches, Crys. Growth Des. 8 (2008) 734-738.

[46] H. Zhang, J. Huang, X. Zhou, X. Zhong, Single-Crystal Bi_2S_3 Nanosheets Growing via Attachment Recrystallization of Nanorods, Inorg. Chem. 50 (2011) 7729–7734.

[47] G. Xie, Z.P. Qiao, M.H. Zeng, X.M. Chen, S.L. Gao, A single-source approach to Bi_2S_3 and Sb_2S_3 nanorods via a hydrothermal treatment, Cryst. Growth Des. 4 (2004) 513–516.

[48] D.C. Onwudiwe, P.A. Ajibade, ZnS, CdS and HgS nanoparticles via alkyl-phenyl dithiocarbamate complexes as single source precursors, Int. J. Mol. Sci 12 (2011a) 5538–5551.

[49] R. Romano, O.L. Alves, Semiconductor/porous silica glass nanocomposites via the single-source precursor approach, Mater. Res. Bull. 41 (2006) 376–386.

[50] R. Nomura, A. Takabe, H. Matsuda, Facile synthesis of antimony dithiocarbamate complexes, Polyhedron 6 (1987) 411–416.

[51] H. Yin, Synthesis, characterizations and crystal structures of new antimony(III) complexes with dithiocarbamate ligands, Polyhedron 27 (2008) 663–670.

[52] N. Awang, I. Baba and B.M. Yamin, Synthesis, characterization and crystal structure of triphenyltin (IV) N-alkyl-N-cyclohexyldithiocarbamate compounds, World Appl. Sci. J. 12 (2011) 630–635.

[53] G.S. Sivagurunathan, K. Ramalingam, C. Rizzoli, Continuous shape measure of electronic effect free steric distortions in tris(dithiocarbamato)indium(III): synthesis,

spectral, electrochemical, single crystal X-ray structural investigations and BVS calculations on tris(dithiocarbamato)indium(III) complexes, Polyhedron 72 (2014) 96–102.

[54] S.T. Breviglieri, E.T.G. Cavalheiro, G.O. Chierice, Correlation between ionic radius and thermal decomposition of Fe(II), Co(II), Ni(II), Cu(II) and Zn(II) diethanoldithiocarbamates, Thermochim. Acta 356 (2000) 79–84.

[55] D.C. Menezes, G.M. de Lima, A.O. Porto, C.L. Donnici, J.D. Ardisson, Synthesis, characterisation and thermal decomposition of tin(IV) dithiocarbamate derivatives – single source precursors for tin sulfide powders, Polyhedron 23 (2004) 2103–2109.

[56] N.L. Pickett, P.O. Brien, Syntheses of semiconductor nanoparticles using single-molecular precursors, Chem. Rec. 1 (2001) 467–479.

[57] S. Thirumaran, K. Ramalingam, Mixed ligand complexes involving amino acid dithiocarbamates, substituted phosphines and nickel(II), Transit. Metal Chem. 25 (2000) 60–62.

[58] D.C. Onwudiwe, P.A. Ajibade, Synthesis, characterization and thermal studies of Zn(II), Cd(II) and Hg(II) complexes of N-Methyl-N-Phenyldithiocarbamate: the single crystal structure of $[(C_6H_5)(CH_3)NCS_2]_4Hg_2$, Int. J. Mol. Sci. 12 (2011b) 1964–1978.

[59] M. Shahid, T. Ruffer, H. Lang, S.A. Awan, S. Ahmad, Synthesis and crystal structure of a dinuclear zinc(II)-dithiocarbamate complex, bis{[(μ^2-pyrrolidinedithiocarbamato-S,S′)(pyrrolidinedithiocarbamato-S,S')zinc(II)]}, J. Coord. Chem. 62 (2009) 440−445.

[60] M. Honda, M. Komura, M. Kawasaki, T.O.R. Tanaka, Infra-red and PMR Spectra of some organo-tin(IV) N, N-Dimethyldithiocarbamates, J. Inorg. Nucl. Chem. 30 (1968) 3231–3237.

[61] R.R. Martínez, R.M. Huicochea, J.A.G. Alvarez, H. Hopfl, H. Tlahuext, Synthesis, heteronuclear NMR and X-ray crystallographic studies of two dinuclear diorganotin(IV) dithiocarbamate macrocycles, Arkivoc v (2008) 19–30.

[62] F. Bonati, U. Renato, Organotin(IV) N,N-disubstituted dithiocarbamates, J. Organomet. Chem. 10 (1967) 257–268.

[63] M. Sarwar, S. Ahmad, S. Ahmad, S. Ali, S.A. Awan, Copper(II) complexes of pyrrolidine dithiocarbamate, Transit. Metal Chem. 32 (2007) 199–203.

[64] I.A. Mustafa, A.A. Taqa, Coordination compounds of tin and bismuth. Complexes of tin(IV) and bismuth(III) with N,N-Dialkyldithiocarbamates, Synth. React. Inorg. Met. –Org. Chem. 31 (2001) 517–526.

[65] C.A. Tsipis, G.E. Manoussakis: ‘Syntheses complexes and spectral study of new iodohis (dialkyldithiocarbamate) of arsenic, antimony and bismuth, Inorg. Chim. Acta 18 (1976) 35–45.

[66] H. Li, C.S. Lai, J. Wu, P.C. Ho, D. de Vos, E.R.T. Tiekink, Cytotoxicity, qualitative structure–activity relationship (QSAR), and anti-tumor activity of bismuth dithiocarbamate complexes, J. Inorg. Biochem. 101 (2007) 809–816.

[67] Y.W. Koh, C.S. Lai, A.Y. Du, E.R.T. Tiekink, Growth of bismuth sulfide nanowire using bismuth trisxanthate single source precursors, Chem. Mater. 15 (2003) 4544–4554.

[68] L. Motevalizadeh, Z. Heidary, M.E. Abrishami, Facile template-free hydrothermal synthesis and microstrain measurement of ZnO nanorods, Bull. Mater. Sci. 37 (2014) 397–405.

[69] R. Chen, M.H. So, C.–M. Che, H. Sun, Controlled synthesis of high crystalline bismuth sulfide nanorods: using bismuth citrate as a precursor, J. Mater. Chem. 15 (2005) 4540–4545.

[70] Y. Gong, Z. Hao, J.L. Sun, H. Shi, P. Jiang, J. Lin, Metal(II) complexes based on 1,4-bis-(3-pyridylaminomethyl)benzene: structures, photoluminescence and photocatalytic properties, Dalton Trans. 42 (2013) 13241–13250.

[71] H. Li, Y. Zhu, S. Chen, O. Palchik, J. Xiong, Y. Koltypin, Y. Gofer, A. Gedanken, A novel ultrasound-assisted approach to the synthesis of CdSe and CdS nanoparticles, J. Solid State Chem. 172 (2003) 102–110.

[72] J. Black, E.M. Conwbll, S. Electric, L. Seigle, C.W. Spencer, Electrical and optical properties of some $M_2^{V-B}N_3^{V1-B}$ semiconductors, J. Phys. Chem. Solids 2 (1957) 240–251.

Figure Captions

Fig. 1. General reaction of bismuth dithiocarbamate.
Fig. 2. FTIR spectrum of bismuth dithiocarbamate.
Fig. 3. Mass spectrum of bismuth dithiocarbamate.
Fig. 4. TGA and DTG thermograms of bismuth dithiocarbamate.
Fig. 5. DSC thermogram of bismuth dithiocarbamate.
Fig. 6. XRD patterns of Bi_2S_3 powder prepared at 400 °C and different calcination duration: (a) 2 h (b) 4 h (c) 6 h.
Fig.7. Electron microscopy images of bismuth sulphide prepared at 400 °C and different calcination duration: (a) 2 h (FESEM), (b) 4 h (FESEM), (c) 6 h (FESEM), (d) 2 h (TEM), (e) 4 h (TEM) and (f) 6 h (TEM).
Fig. 8. Images of particle size distribution of bismuth sulphide prepared at 400 °C and different calcination duration: (a) 2 h (TEM), (b) 4 h (TEM), (c) 6 h (TEM).
Fig. 9. EDX spectra of bismuth sulphide prepared at 400 °C and different calcination duration: (a) 2 h (b) 4 h (c) 6 h.
Fig. 10. Kubelka–Munk transformed reflectance spectra of bismuth sulphides prepared at 400 °C and different calcination duration: (a) 2 h (b) 4 h (c) 6 h.

Table 1 Physical and elemental analysis of bismuth dithiocarbamate

Compound (Formula Weight) (g/mol)	Yield (%)	Colour	Elemental Analysis %Found (Calc.)				
			C	H	N	S	Bi
$C_{27}H_{48}N_3S_6Bi$ (815)	96	Yellowish Orange	38.48 (39.74)	5.48 (5.93)	5.13 (5.15)	24.28 (23.58)	25.61 (25.99)

Table 2 Selected mass spectral fragments for bismuth dithiocarbamate

Probable ion	Value of molecular ion peak, m/z
$[Bi(S_2CNC_8H_{16})_3]^{+\bullet}$	....
$[Bi(S_2CNC_8H_{16})_2]^+$	613
$[BiS_2CNC_8H_{16}]^+$	411
$[C_8H_{16}NCS]^+$	170
$[C_3H_6NS]^+$	88
$[C_4H_7]^+$	55

Table 3 Thermal analysis of bismuth dithiocarbamate

Compound	DSC peak (°C)	DTG Max value (°C)	Decomposition Temperature (°C)	Percentage weight loss (%) Found (Calc.)	Percentage residue (%) Found (Calc.)	Residue expected
$C_{27}H_{48}N_3S_6Bi$	127	122	76-192	11.69(10.67)	31.62(31.53)	Bi_2S_3
	157	307	211-346	56.69(57.80)		
	178					
	292					
	304					

Table 4 Crystallite and mean particle sizes of bismuth sulphide

Sample	Duration of calcination (hour)	Average Crystallite sizes, t (nm)	Mean Particle width (nm)
Bi_2S_3 (2 h)	2	21.03	29.35
Bi_2S_3 (4 h)	4	23.79	29.76
Bi_2S_3 (6 h)	6	25.58	35.95

Figure 1

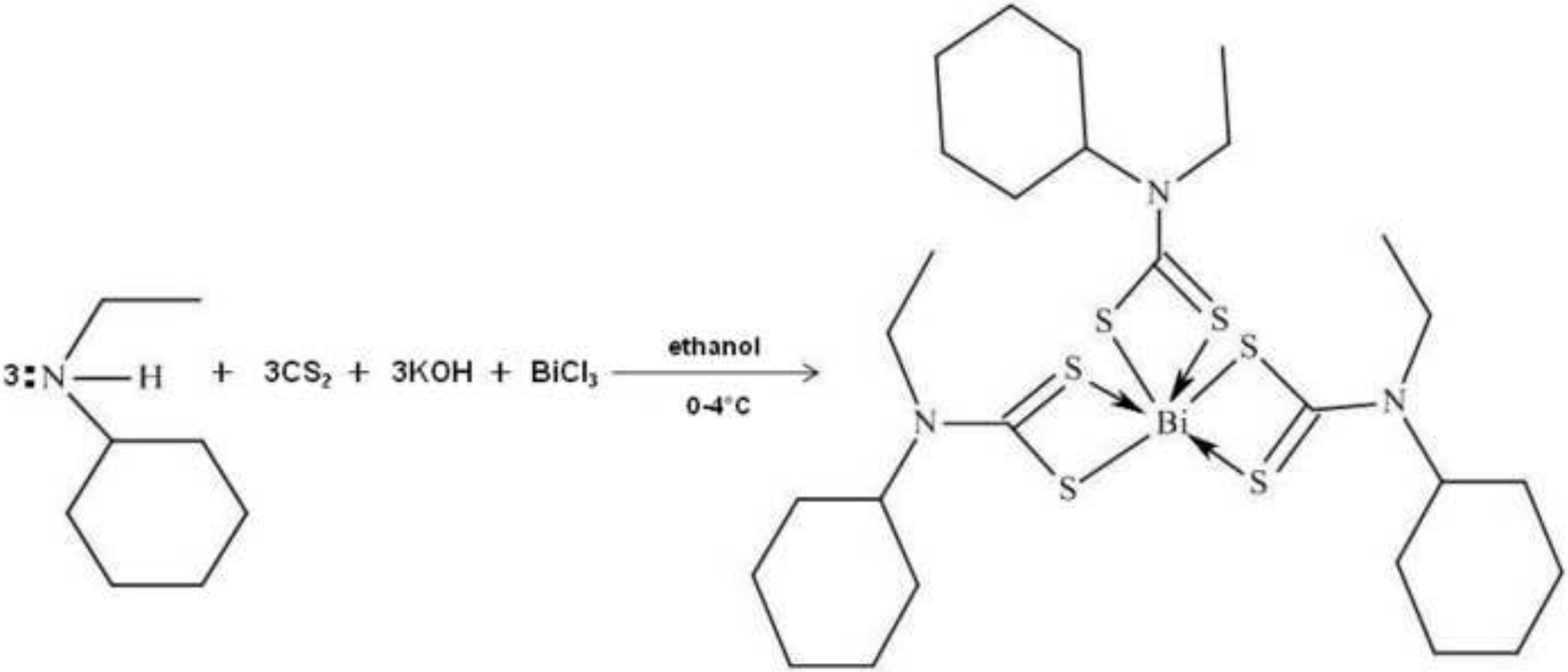

Figure 2

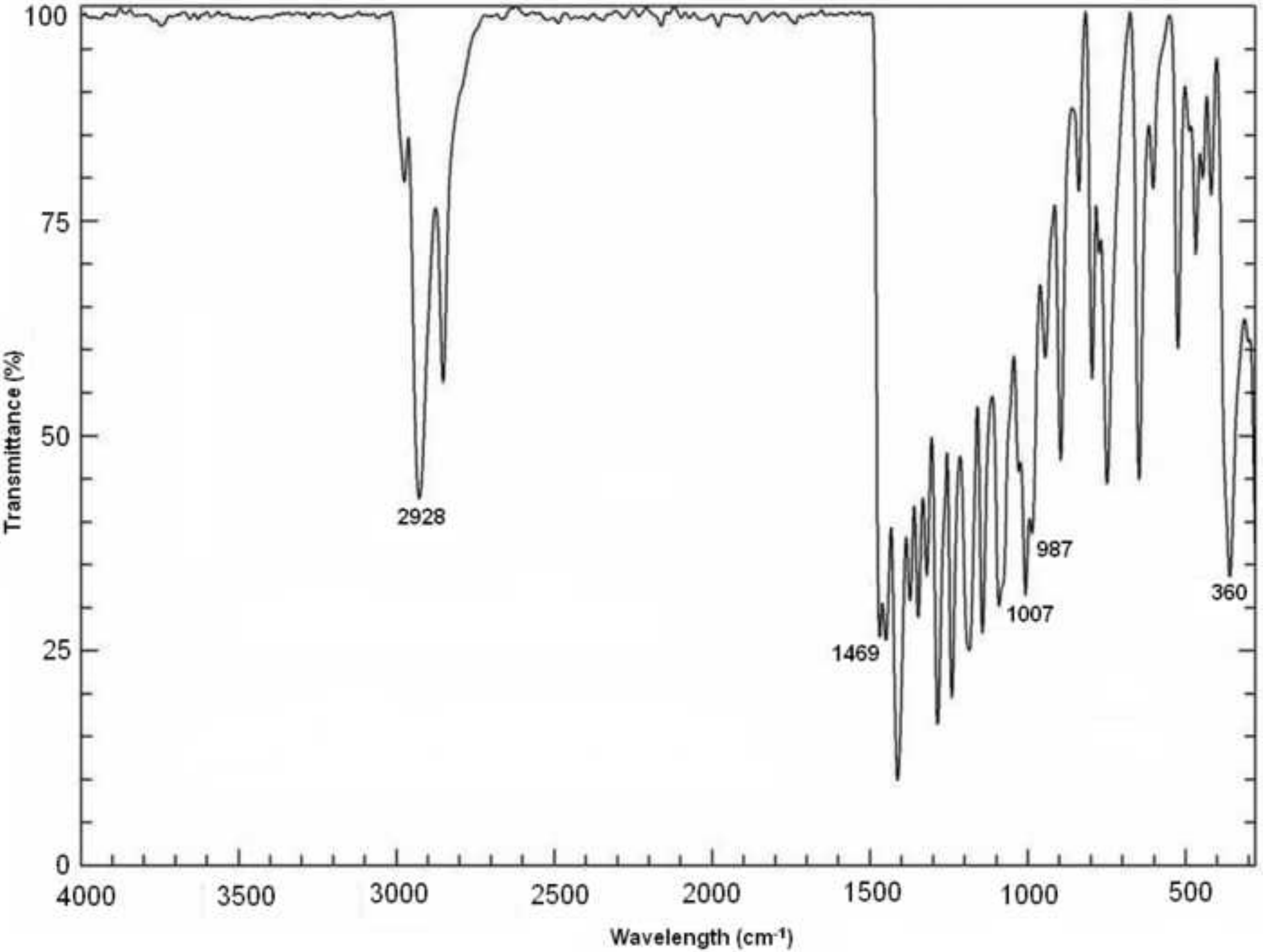

100
75
50
25
0
Transmittance (%)
2928
1469
1007
987
360
4000
3500
3000
2500
2000
1500
1000
500
Wavelength (cm-1)

Figure 3

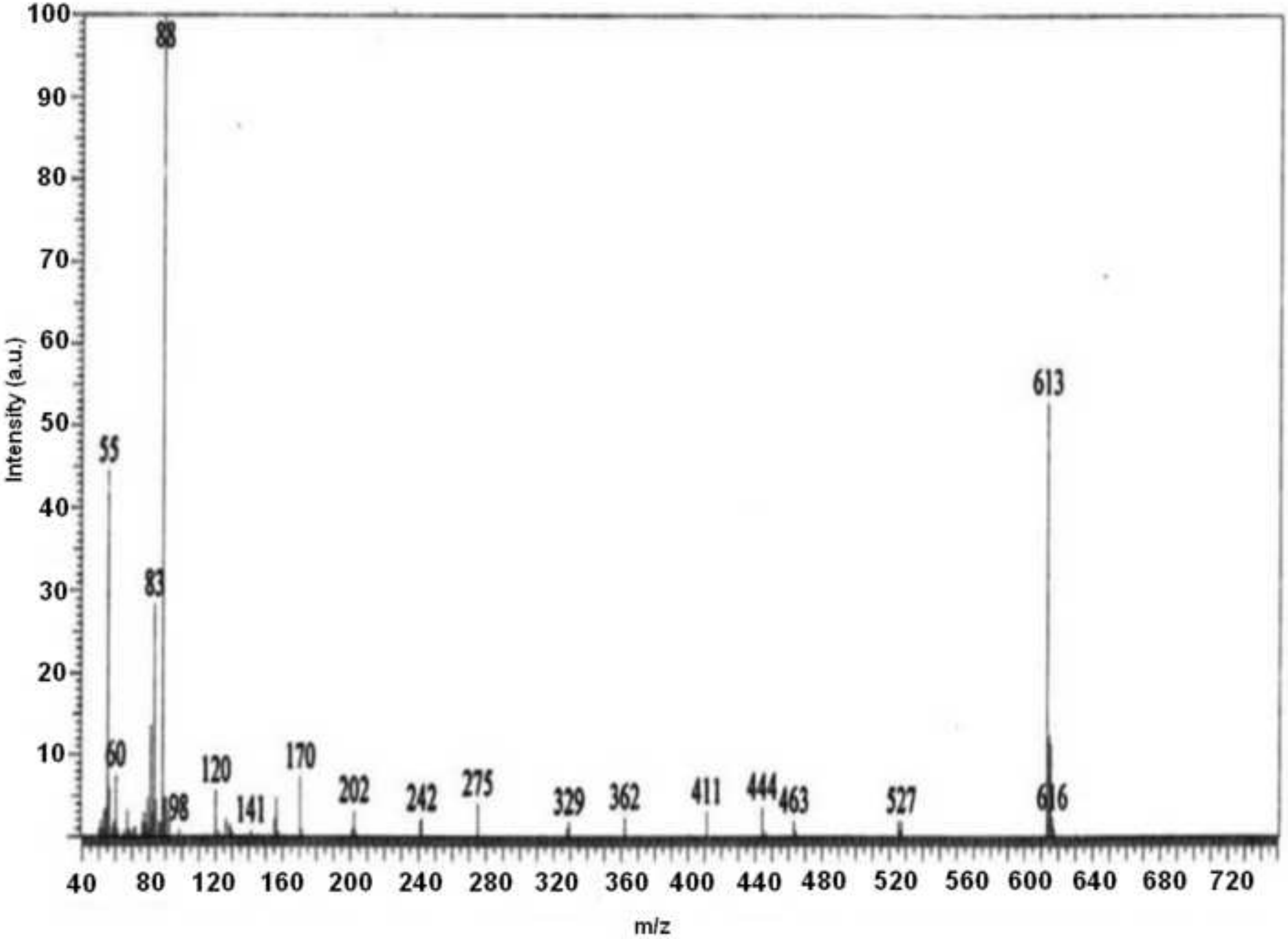
Intensity (a.u.)
100
90
80
70
60
50
40
30
20
10
m/z
40
80
120
160
200
240
280
320
360
400
440
480
520
560
600
640
680
720
88
613
55
83
60
98
120
141
170
202
242
275
329
362
411
444
463
527
616

Figure 4

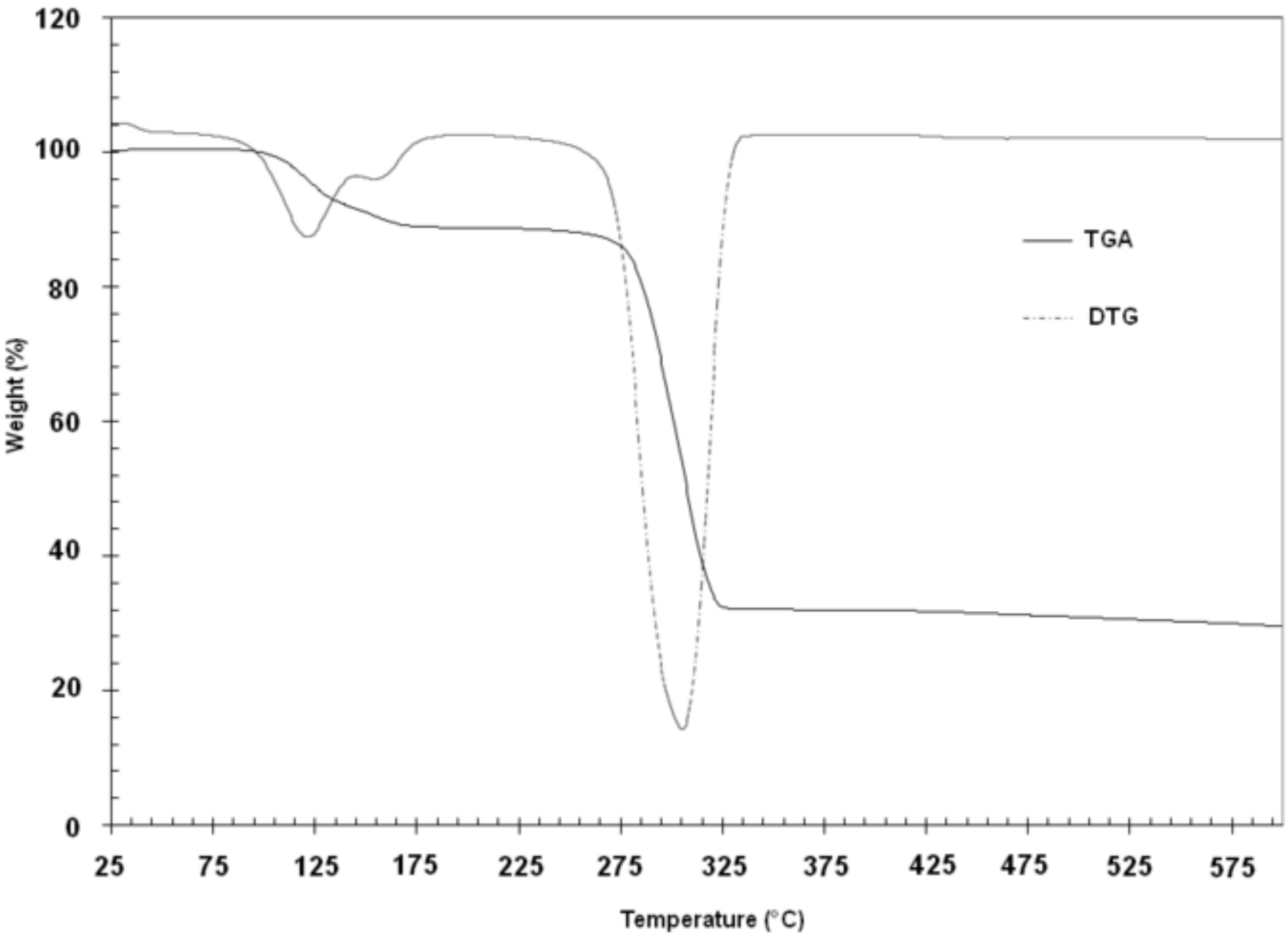

120
100
80
60
40
20
0
Weight (%)
25
75
125
175
225
275
325
375
425
475
525
575
Temperature (°C)
TGA
DTG

Figure 5

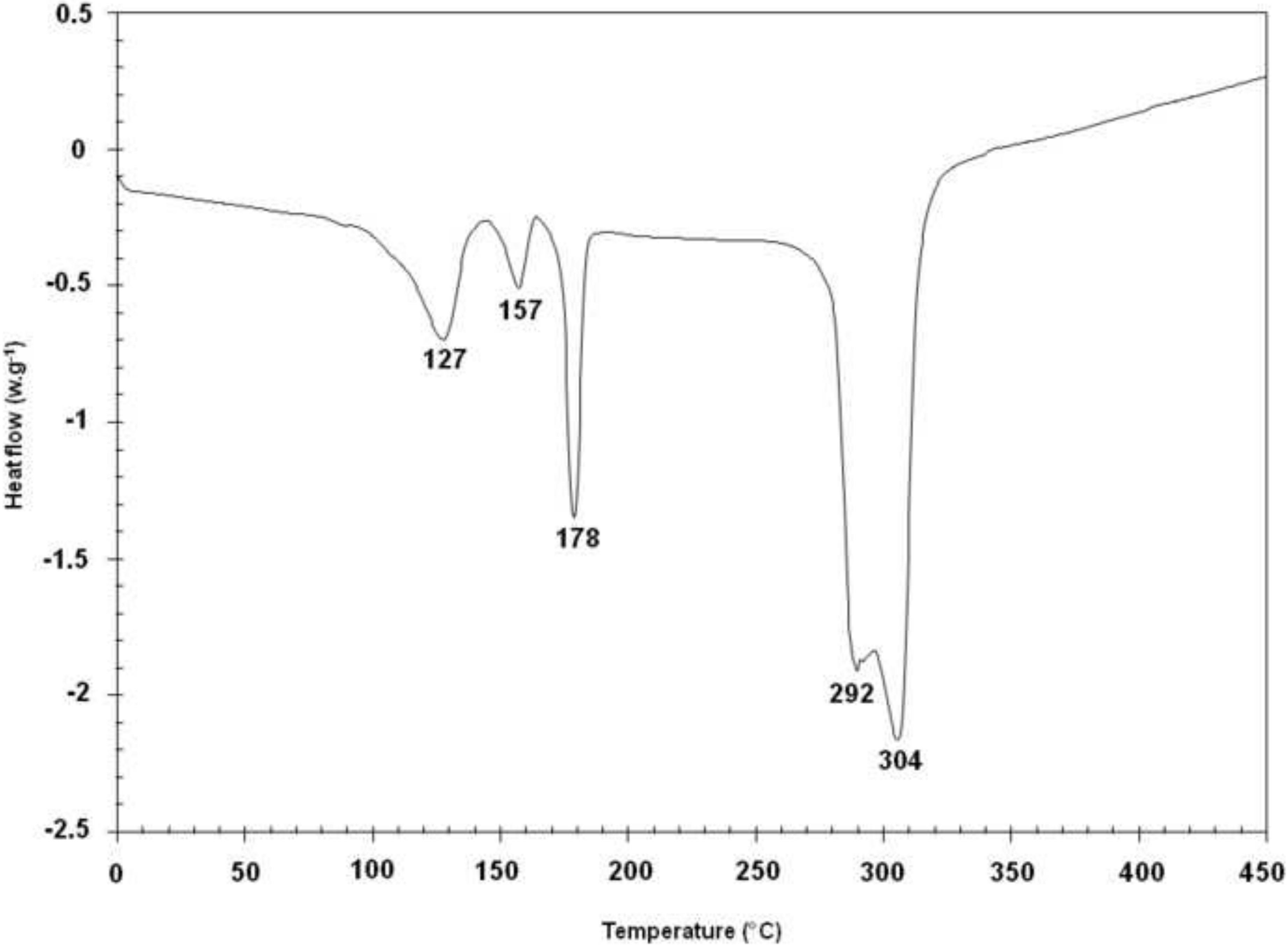
0.5
0
-0.5
-1
-1.5
-2
-2.5
Heat flow (w.g^{-1})
0
50
100
150
200
250
300
350
400
450
Temperature (°C)
127
157
178
292
304

Figure 6

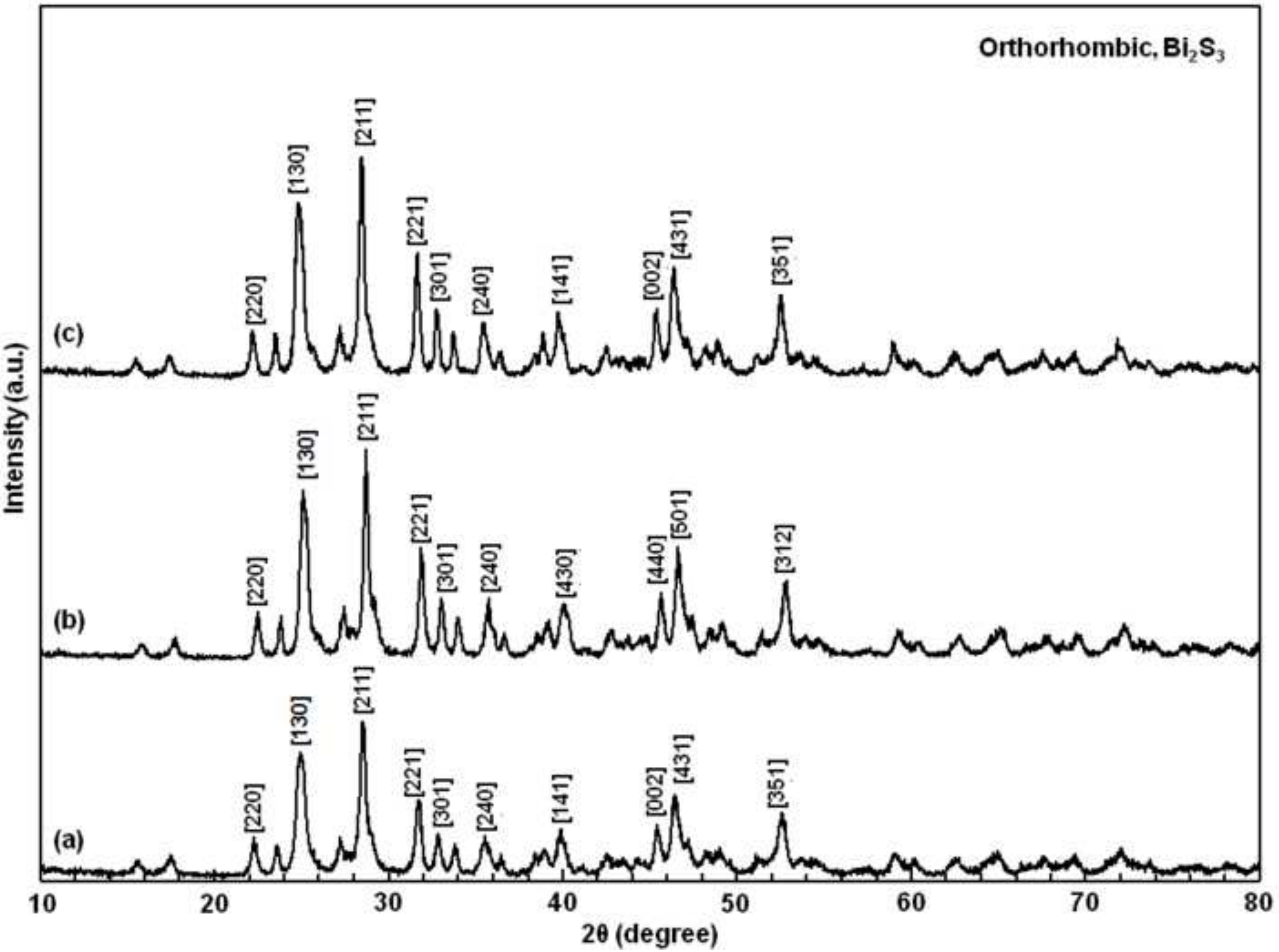

Orthorhombic, Bi_2S_3
(c)
[220]
[130]
[211]
[221]
[301]
[240]
[141]
[002]
[431]
[351]
(b)
[220]
[130]
[211]
[221]
[301]
[240]
[430]
[440]
[501]
[312]
(a)
[220]
[130]
[211]
[221]
[301]
[240]
[141]
[002]
[431]
[351]
Intensity (a.u.)
10
20
30
40
50
60
70
80
2θ (degree)

Figure 7(a)

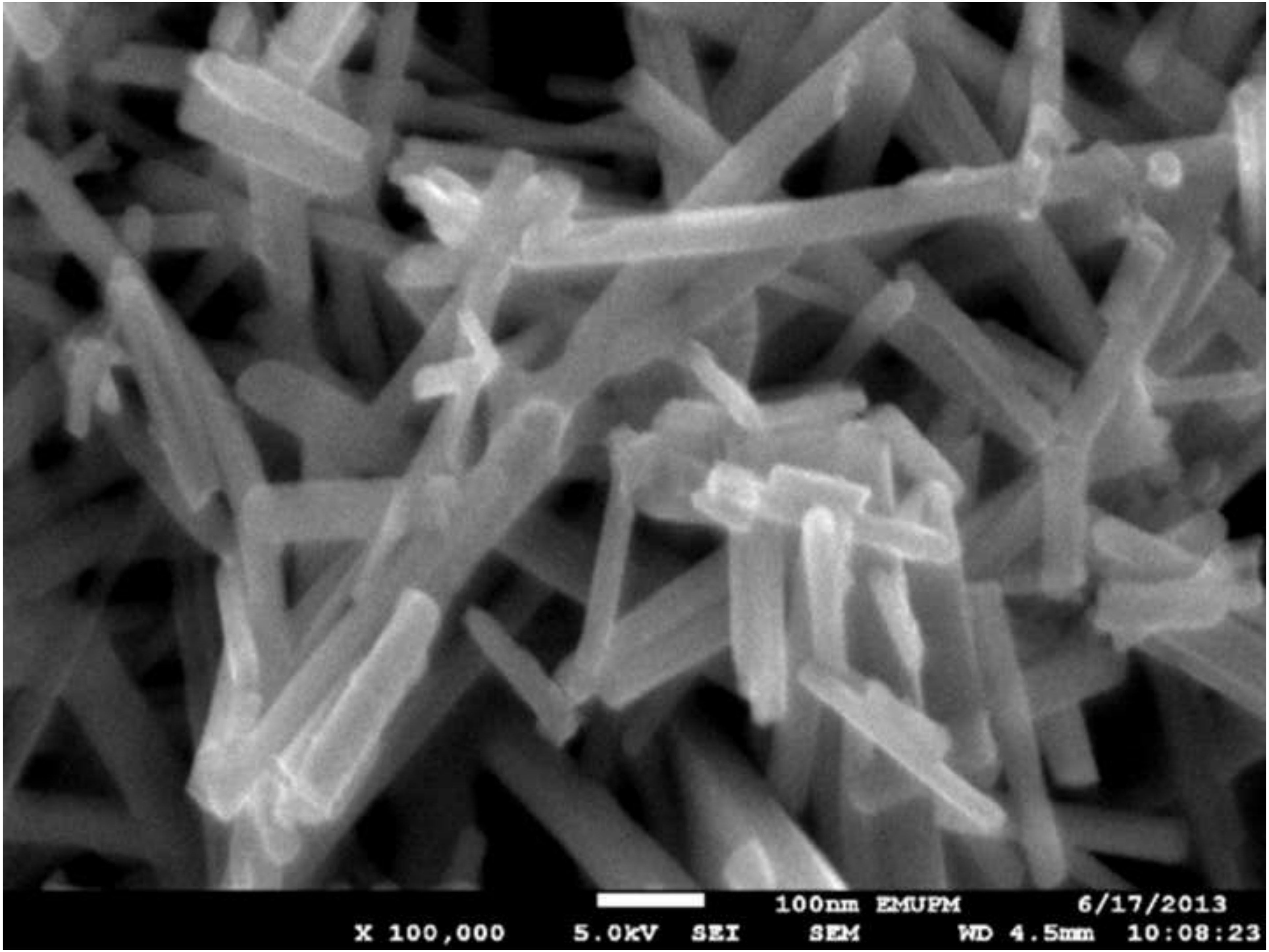

Figure 7(b)

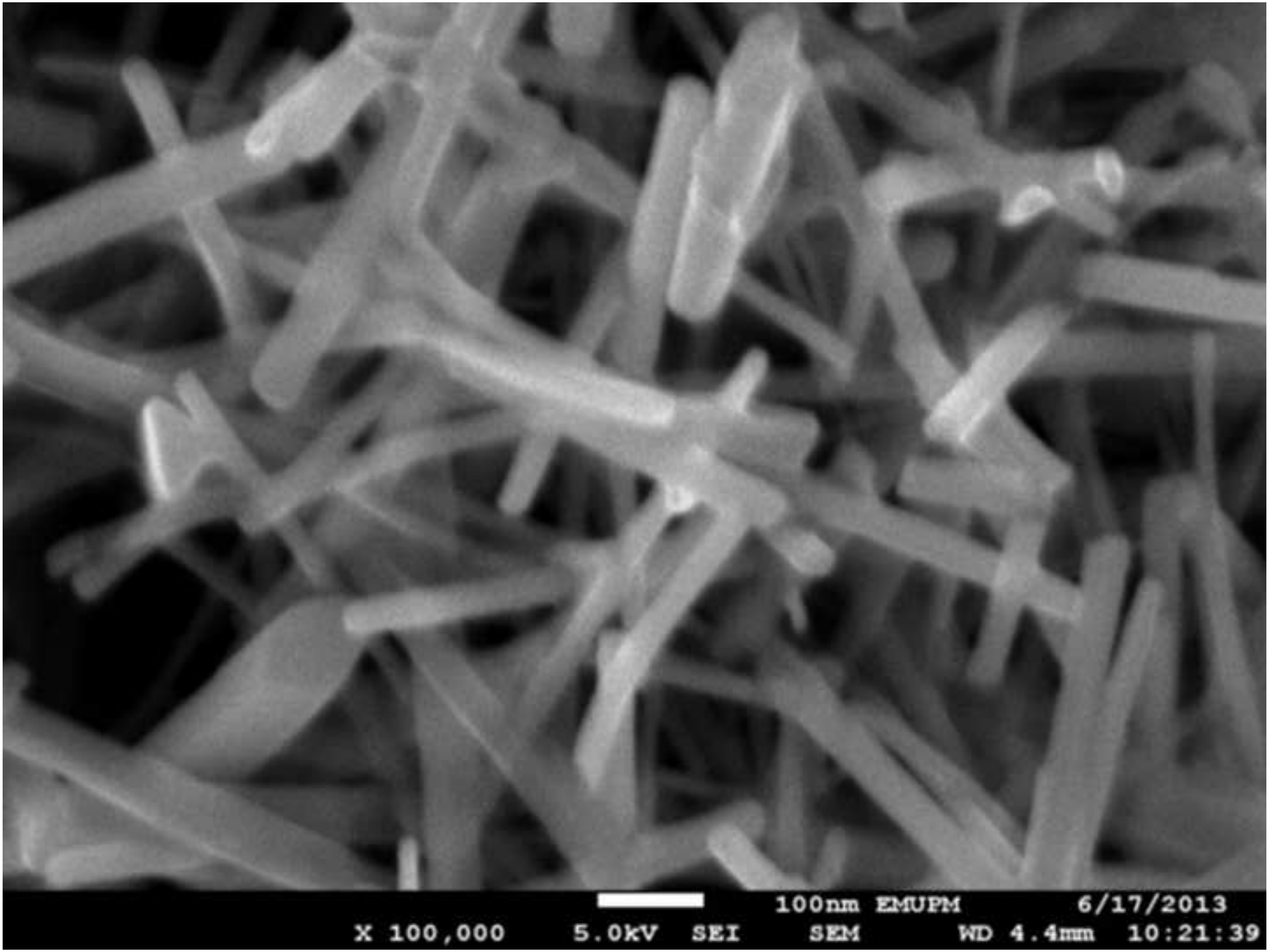

Figure 7(c)

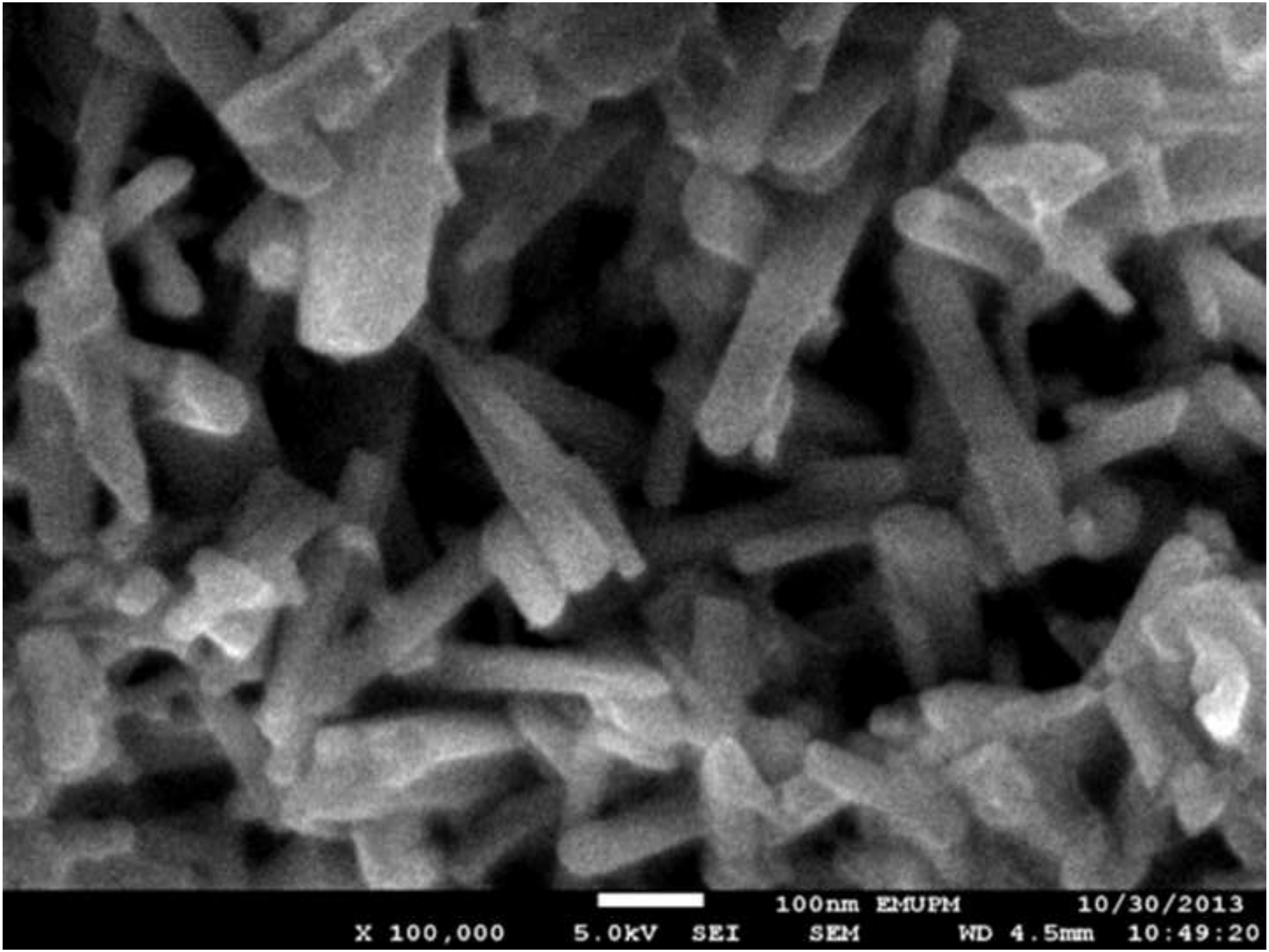

Figure 7(d)

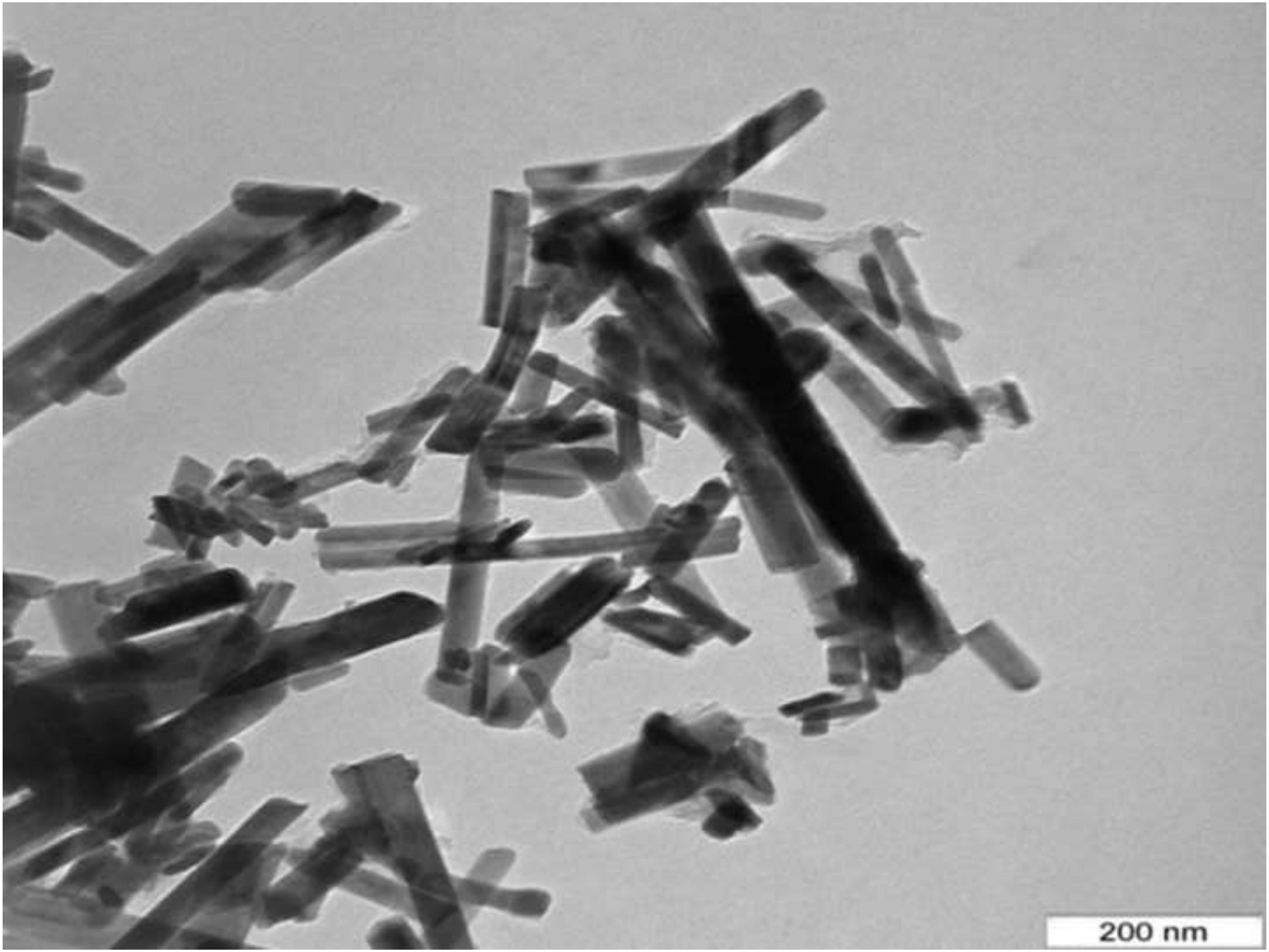

Figure 7(e)

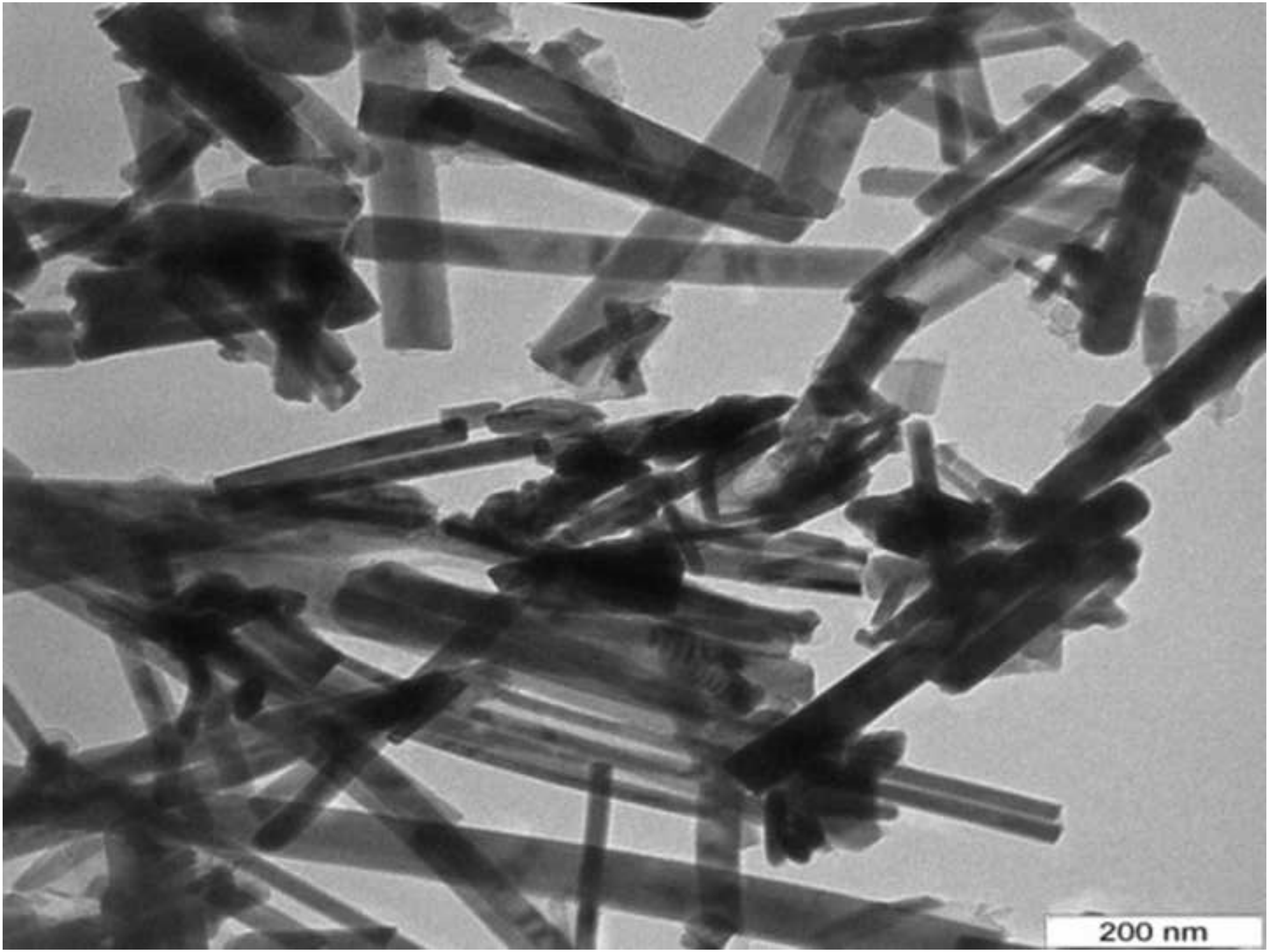

Figure 7(f)

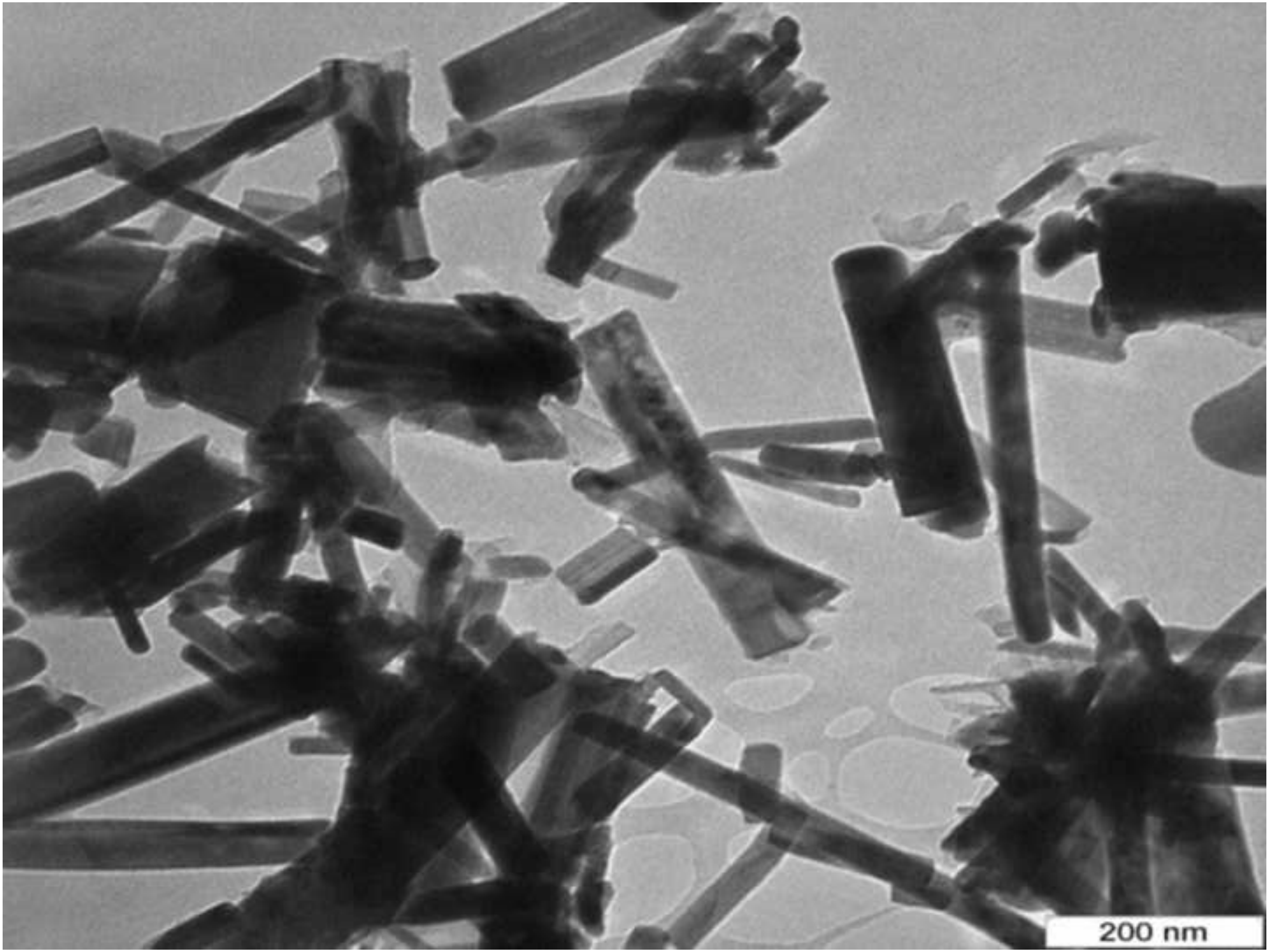

Figure 8(a)

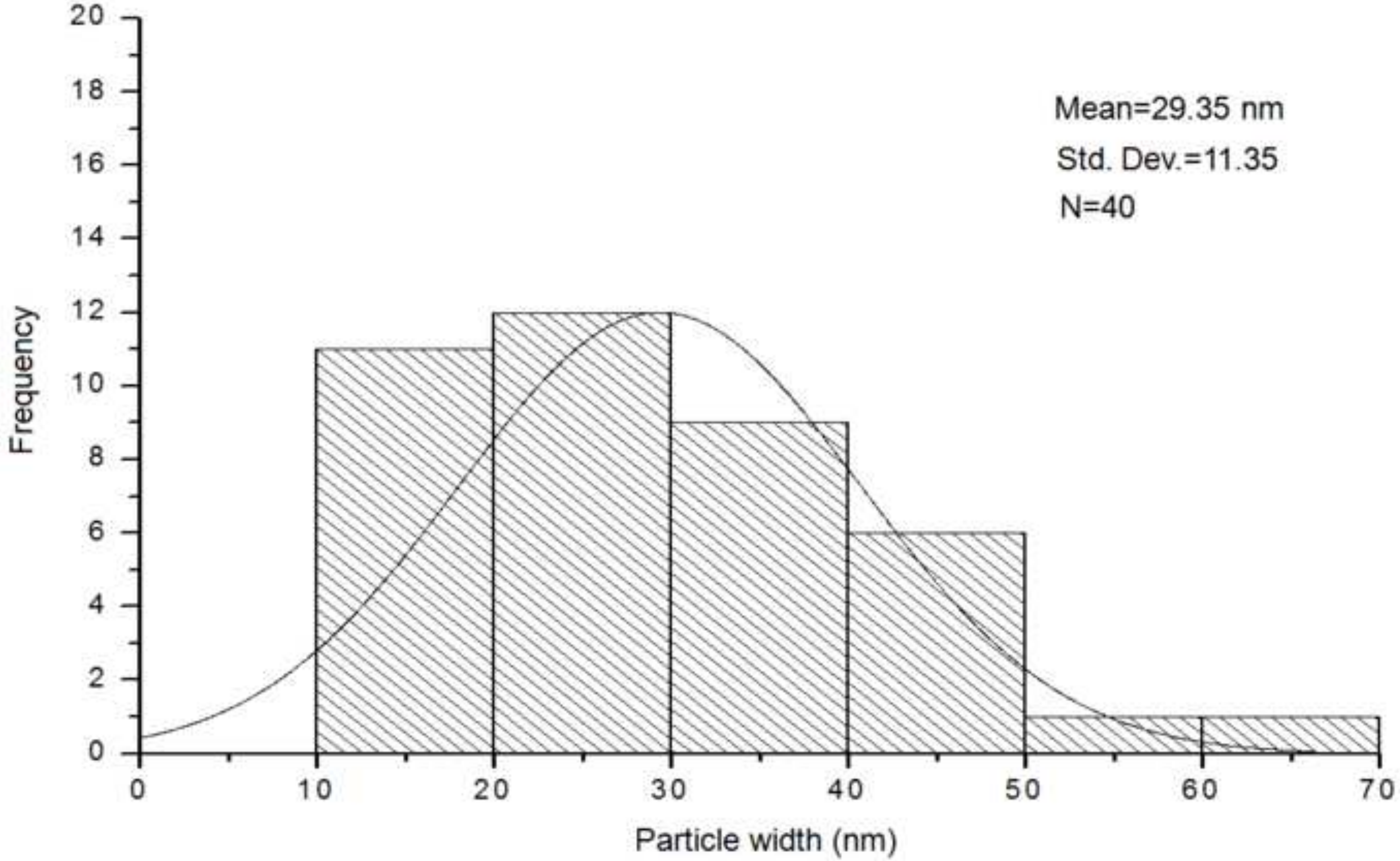
Mean=29.35 nm
Std. Dev.=11.35
N=40
Frequency
0
2
4
6
8
10
12
14
16
18
20
0
10
20
30
40
50
60
70
Particle width (nm)

Figure 8(b)

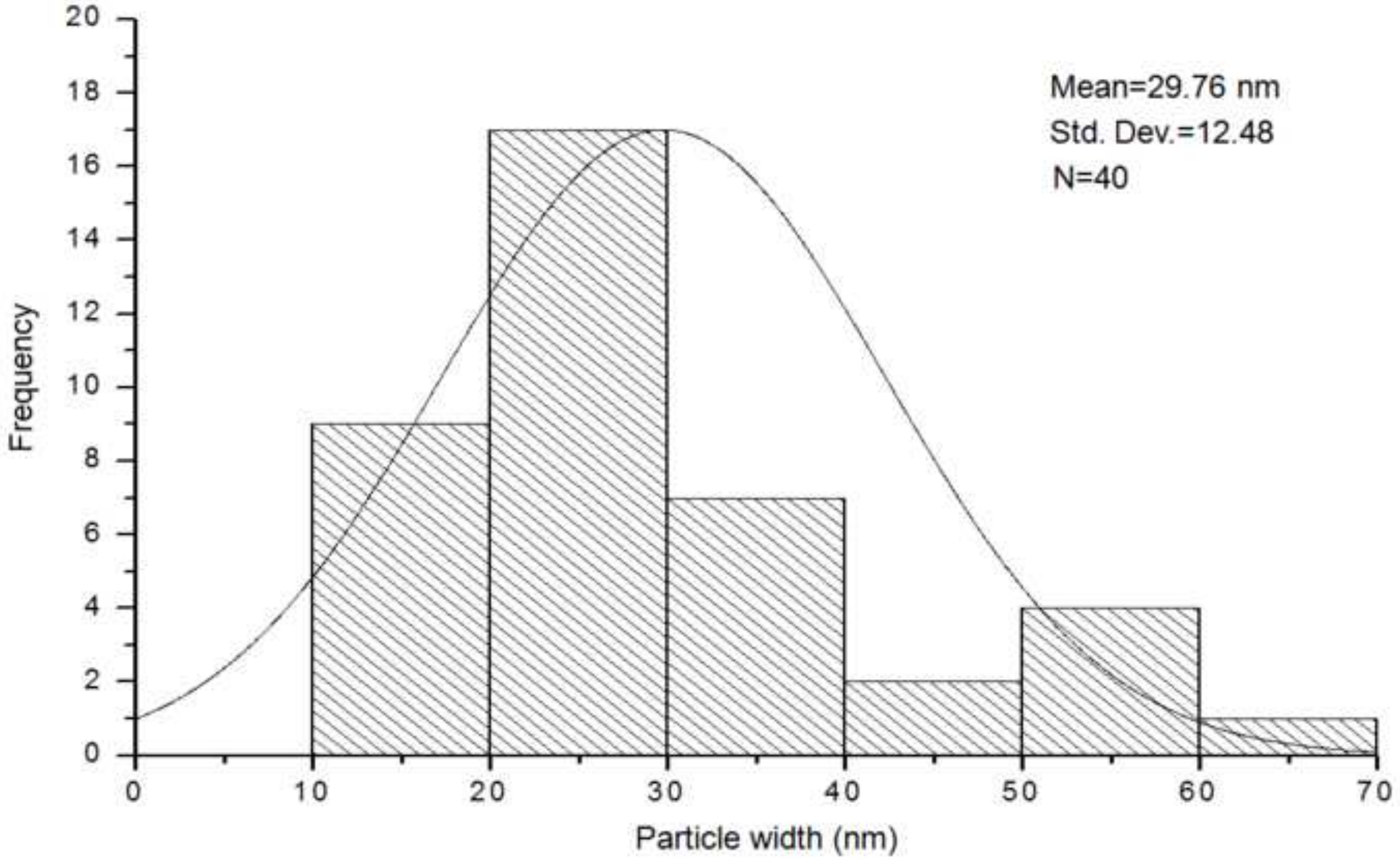
Mean=29.76 nm
Std. Dev.=12.48
N=40
Frequency
0
2
4
6
8
10
12
14
16
18
20
0
10
20
30
40
50
60
70
Particle width (nm)

Figure 8(c)

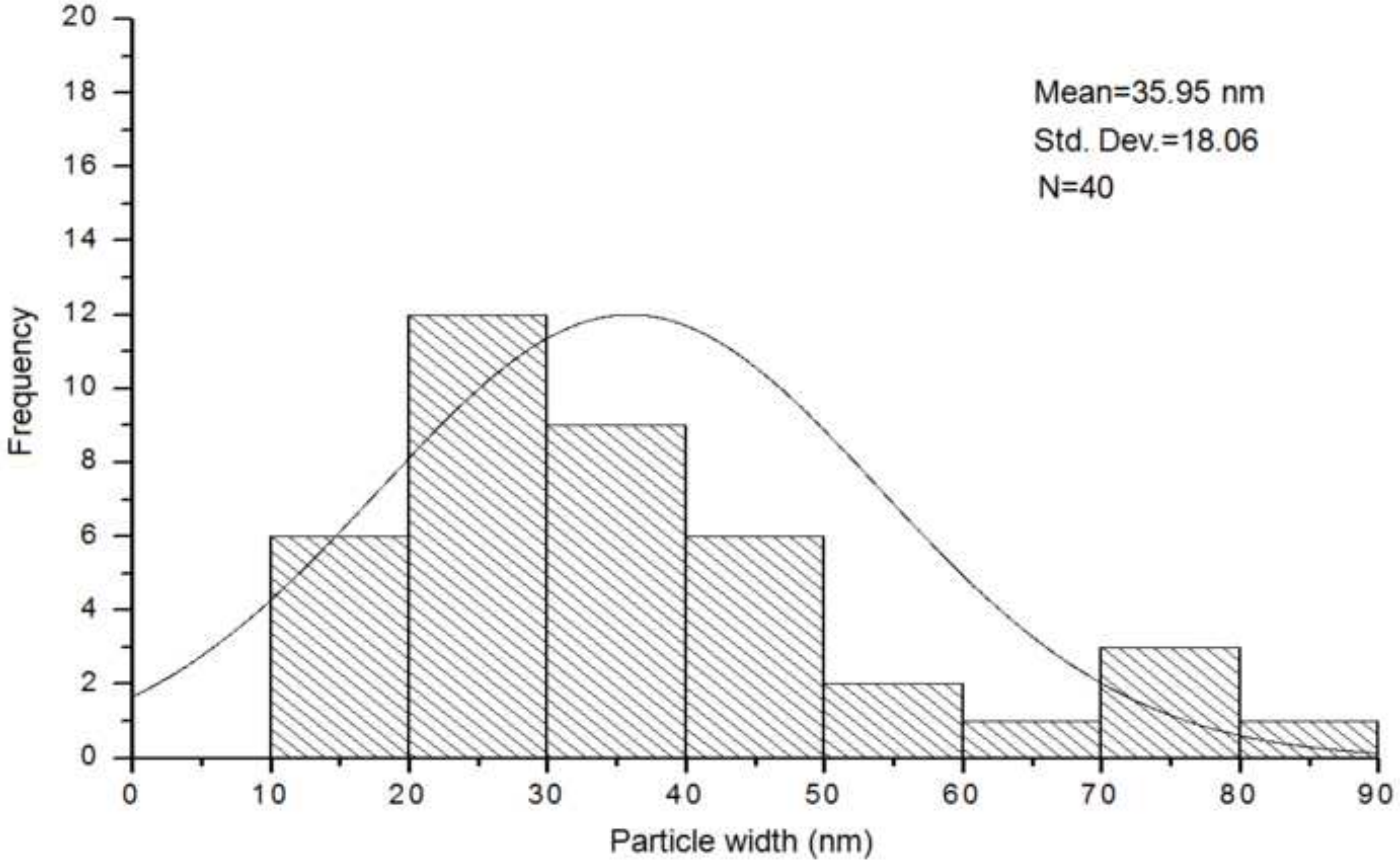
Mean=35.95 nm
Std. Dev.=18.06
N=40
Frequency
0
2
4
6
8
10
12
14
16
18
20
0
10
20
30
40
50
60
70
80
90
Particle width (nm)

Figure 9(a)

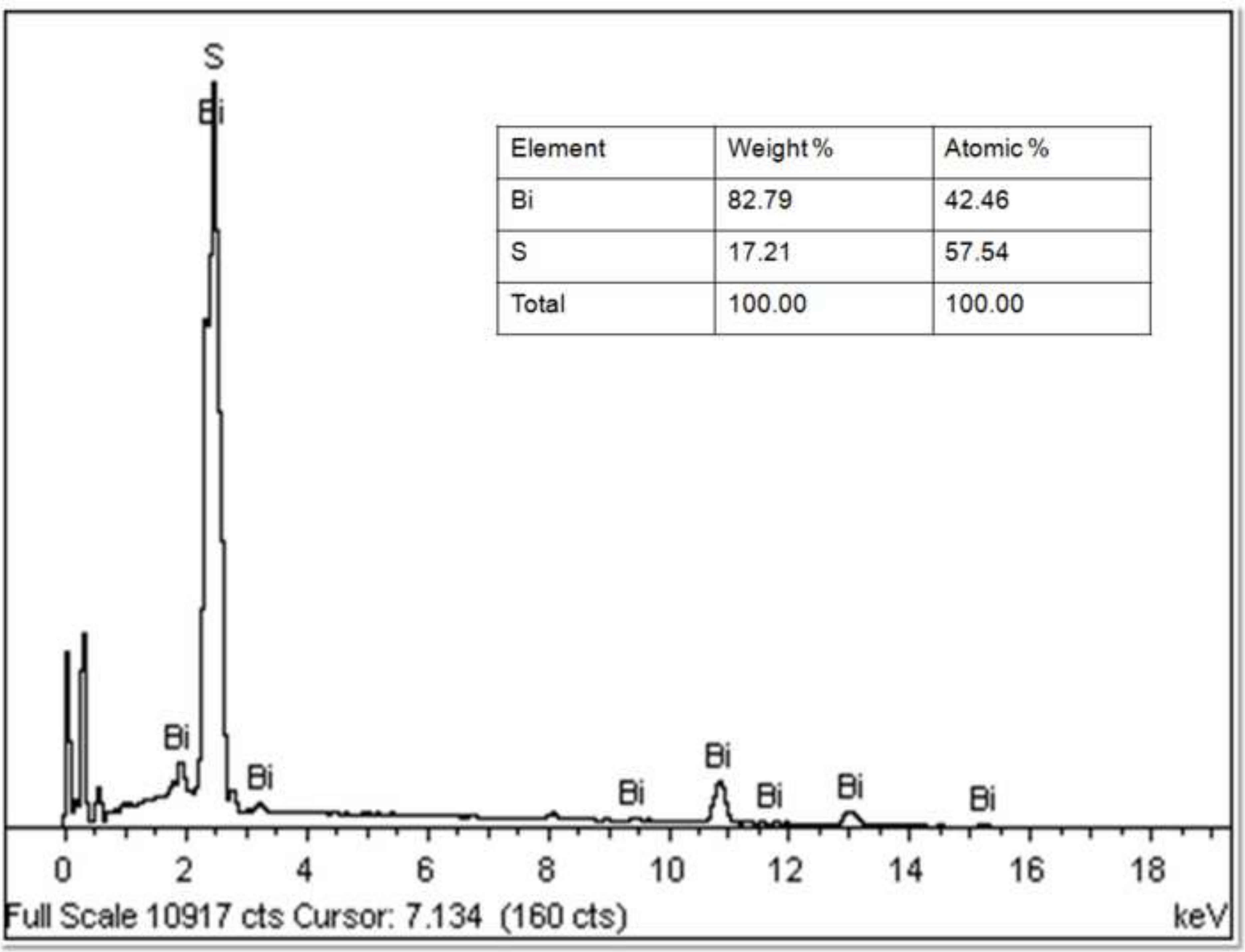

Element	Weight %	Atomic %
Bi	82.79	42.46
S	17.21	57.54
Total	100.00	100.00

Figure 9(b)

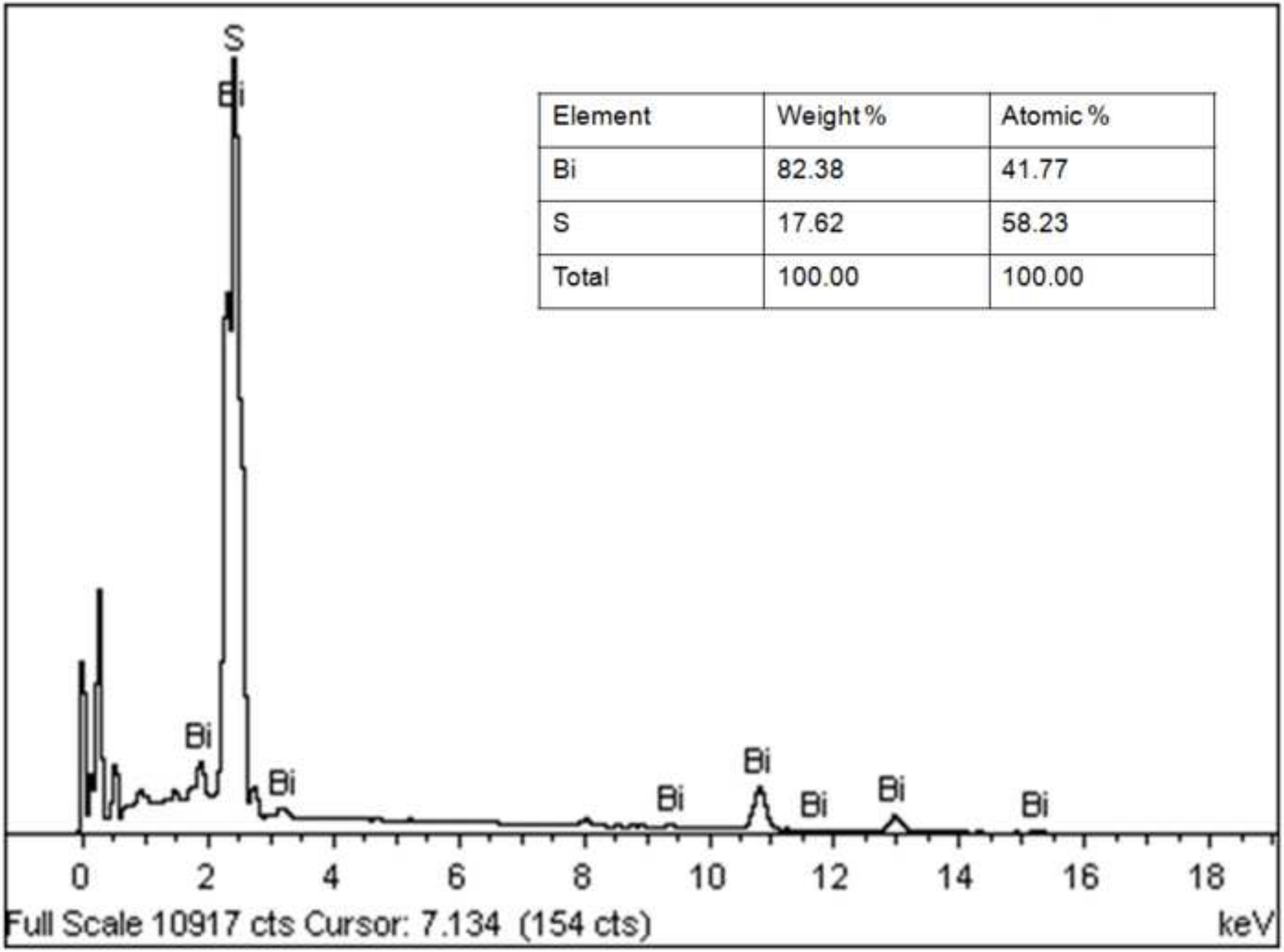

Element	Weight %	Atomic %
Bi	82.38	41.77
S	17.62	58.23
Total	100.00	100.00

Figure 9(c)

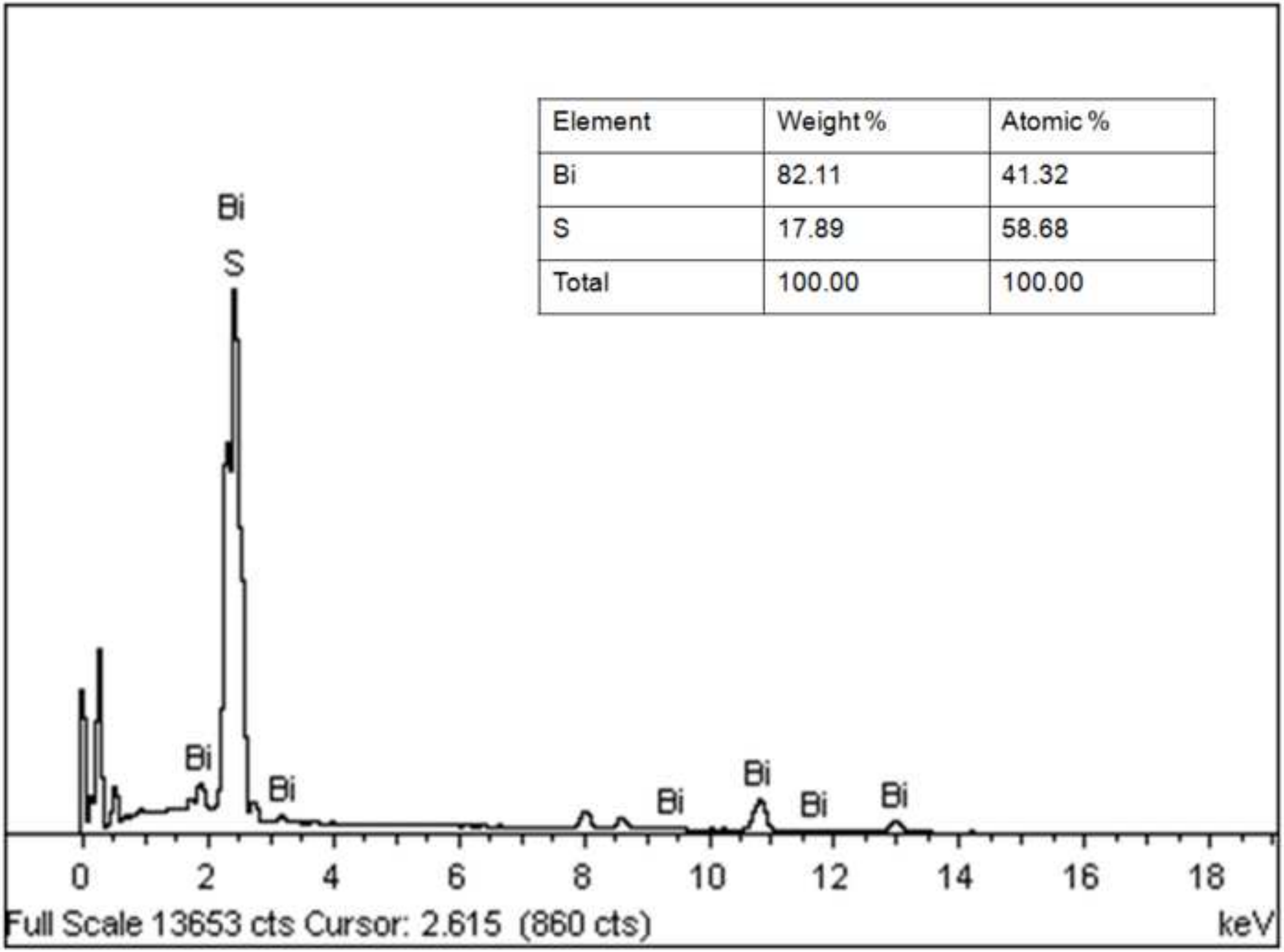

Element	Weight %	Atomic %
Bi	82.11	41.32
S	17.89	58.68
Total	100.00	100.00

Figure 10